Backbending region study in ^{160,162}Dy using incomplete fusion reactions

A. Jungclaus
Instituto de Estructura de la Materia, Consejo Superior de Investigaciones Científicas, E-28006 Madrid, Spain and Universidad Autónoma de Madrid, E-28049 Madrid, Spain

B. Binder, A. Dietrich, T. Härtlein, H. Bauer, Ch. Gund, D. Pansegrau, and D. Schwalm
Max-Planck-Institut für Kernphysik, D-69029 Heidelberg, Germany

J. L. Egido
Departamento de Fisica Teórica, Universidad Autónoma de Madrid, E-28049 Madrid, Spain

Y. Sun
Department of Physics and Astronomy, University of Tennessee, Knoxville, Tennessee 37996

D. Bazzacco, G. de Angelis, E. Farnea, A. Gadea, S. Lunardi, D. R. Napoli, C. Rossi-Alvarez, and C. Ur
Istituto Nazionale di Fisica Nucleare, Laboratori Nazionali di Legnaro, I-35020 Legnaro, Italy and Dipartimento di Fisica dell' Università di Padova, Padova, Italy

G. B. Hagemann
Niels Bohr Institute, DK-2100 Copenhagen, Denmark
(Received 1 March 2002; published 26 July 2002)

The incomplete fusion reactions ^{7}Li$\rightarrow^{158,160}$Gd at beam energies of 8 MeV/nucleon have been used to study the first band crossing region in the heavy stable Dy isotopes ^{160,162}Dy. The γ rays were detected in the GASP spectrometer in coincidence with fast charged particles detected in the ISIS silicon ball. We succeeded to observe the first backbending in ^{162}Dy at a crossing frequency of $\hbar\omega \approx 350$ keV, a value much higher than expected from other nuclei in this mass region. Moreover, for the first time in a nucleus with a very large interaction strength, the yrare band in ^{160}Dy could be established up to rather high spin ($I=20\hbar$) allowing for a precise determination of the interaction strength between the ground state and the Stockholm band, $|V_{g\text{-}S}| = 219(2)$ keV. Together with $|V_{g\text{-}S}| = 14(2)$ keV determined for the corresponding interaction in ^{162}Dy, a full oscillation of the strengths from one node to the next could be observed within an isotopic chain. In addition to the ground state and Stockholm bands, many other known bands in the two nuclei were considerably extended to higher spin and the experimental results are compared to calculations within the projected shell model.

DOI: 10.1103/PhysRevC.66.014312 PACS number(s): 23.20.Lv, 23.20.En, 27.70.+q, 21.60.Cs

I. INTRODUCTION

Since the pioneering work by the Stockholm group in the 1970s, the first backbending in the yrast sequence of deformed nuclei in the rare earth region is understood as being due to the crossing between the ground state band (g.s.b.) and a rotational band, called the Stockholm band, built on an aligned $i_{13/2}$ neutron pair. Theoretical studies of the interaction strength between these two bands using both the cranking model [1,2] and the particle-rotor model [3–5] predicted that this strength would be an oscillating function of the degree of filling of the high-j subshell. Until now, it was not possible to observe a full period of such an oscillation within one isotopic chain. The reason is a purely experimental one. To determine the interaction strength $|V|$ with reasonable accuracy, it is necessary to observe both interacting bands before and after the crossing. Whereas the neutron deficient isotopes in the rare earth region can be easily populated in heavy-ion fusion-evaporation reactions, in which both the yrast and yrare bands can be observed over a wide spin range, the stable isotopes are usually investigated using multiple Coulomb excitation (MCE) and in this reaction excited states are populated in a more selective way. In the Dy chain, e.g., the isotopes with $A=154,156,158$ have been studied in (HI,xn) reactions, whereas the heavier isotopes with $A=160,162,164$ have been investigated using MCE. It was the main goal of the present work to obtain information about the yrare bands in the band crossing regions of the stable nuclei ^{160,162}Dy in order to deduce accurate interaction strengths and to demonstrate a full oscillation of the strength within a single isotopic chain. We employed the incomplete fusion mechanism which has previously been shown to populate high-spin states in neutron-rich nuclei with rather high cross sections [6–8]. In incomplete fusion, also called massive transfer, the projectile does not completely fuse with the target nucleus but rather breaks up, one fragment flying away without interaction and the other one fusioning with the target nucleus, leading to the final reaction product after the evaporation of some neutrons. The experimental signatures of this reaction are the observation of strongly forward-peaked charged particles (mostly protons, deuterons, and tritons if ^{7}Li is used as a projectile) with much higher energies

than observed in conventional fusion-evaporation reactions. These charged particles can be used for a very efficient channel selection. The incomplete fusion of the ^{7}Li beam with a neutron-rich stable target and the observation of a fast proton is equivalent to a fusion-evaporation reaction with a neutron-rich radioactive ^{6}He beam.

The yrast lines of the even-even Dy isotopes have been studied in detail in the frame of the projected shell model (PSM) in [9,10]. In the present work, we extended these PSM calculations in order to describe in addition excited bands of both parities, for which new experimental information were obtained.

The paper is organized as follows. In Sec. II, details about the two incomplete fusion experiments performed in the present study are given. The conclusions drawn from these experiments regarding the reaction mechanism and the experimental cross sections are discussed in Sec. III. In Sec. IV, first the data analysis procedure and the extended level schemes of ^{160,162}Dy are presented. Then the experimental interaction strengths between the ground state, and the Stockholm and γ bands are determined using a simple two-band-mixing model. In the last part of the paper (Sec. V), the band structures of ^{160}Dy and ^{162}Dy are compared to calculations within the projected shell model. Parts of this work have already been published in conference proceedings [11,12].

II. EXPERIMENTS

Two complementary experiments were performed. The aim of the first experiment, carried out at the Max-Planck-Institut für Kernphysik in Heidelberg, was to measure absolute cross sections for the different channels in the reaction ^{160}Gd+^{7}Li in the beam energy range from 35 to 67 MeV, i.e., excitation functions, in order to determine the optimal beam energy for the population of ^{162}Dy. A 3-mg/cm^2-thick ^{160}Gd foil was used as target and the setup consisted of seven Ge detectors, an ΔE-E Si ring telescope ($d_{\Delta E}$ $=100$ μm, $d_E=1000$ μm, $\Theta=27°$–$37°$) in the forward direction and a 300-μm Si detector in the backward direction. A 470-μm Al absorber was mounted in front of the ΔE detector to protect it against elastically scattered ^{7}Li ions. This experiment is discussed in detail in [13].

In the second experiment, the reactions ^{158,160}Gd (^{7}Li,$(p,d,t)xn$) at a beam energy of 56 MeV were employed to populate high-spin states in the band crossing region of the heavy even Dy isotopes ^{160,162}Dy. The ^{7}Li beam delivered by the XTU tandem accelerator of the Laboratori Nazionali di Legnaro (LNL) was directed onto targets with thicknesses of 3.7 mg/cm^2 (^{158}Gd) and 3.9 mg/cm^2 (^{160}Gd) and the γ radiation was detected in the 40 Compton-suppressed Ge detectors of the GASP array [14] and the 80-element BGO inner ball. In addition, charged particles were detected in the Si ball ISIS [15] consisting of 40 Si ΔE-E telescopes arranged in the same geometry as the Ge crystals in GASP, namely, seven rings with $\Theta=35°$, $59°$, $72°$, $90°$, $108°$, $121°$, and $145°$. To protect the Si detectors from damage by scattered beam particles, an absorber tube consisting of 100-μm Cu and 12-μm Al was mounted around the beam axis. All events with at least three coincident γ rays in the Ge detectors, or two γ rays in the Ge detector plus one particle detected in the Si ball were recorded on tape with the additional condition that the γ multiplicity in the BGO ball was 3 or higher. More details about this experiment are given in [16].

III. THE REACTION MECHANISM

To determine the beam energy best suited to populate the isotopes of interest, the absolute cross sections for the individual reaction products observed in our Heidelberg experiment have been determined for six different beam energies between 35 and 67 MeV. In a first step, relative cross sections were deduced by measuring the total γ flux into the ground states of the different nuclei in the $\gamma\gamma$ coincidence data. The intensities of all γ transitions have been corrected for the energy dependent efficiency of the detectors and internal conversion. For both pure neutron and charged-particle channels, the intensities were deduced without the charged-particle condition. Whereas the γ flux into the ground state is easily determined for the even Dy isotopes, especially in the cases of the Ho nuclei, the complicated band structures as well as isomeric states, blocking part of the γ flux, have to be taken into account very carefully. To determine absolute cross sections from the relative ones, the intensities of the x rays from the Gd target observed in a Ge detector without an absorber have been used. However, since no measurements of x-ray cross sections are available for the reaction ^{7}Li on ^{160}Gd, values calculated using the plane wave Born approximation corrected for binding energy and Coulomb deflection [17] were used. This model has been tested by comparing the calculated values to the experimental cross sections obtained for the reactions ^{7}Li on different targets between Ti (Z $=22$) and Sb ($Z=51$) with beam energies between 1 and 5 MeV/amu in [18]. The calculated and measured values agreed within 20%, so using these calculations to determine absolute cross sections will allow to estimate the cross sections with uncertainties of about 20%. The final values, obtained at the end of this procedure, are shown in Fig. 1(a) for the xn channels leading to the Ho isotopes and in Fig. 1(b) for the charged-particle channels $^{160-164}$Dy and ^{160}Gd.

Whereas the $4n$ to $7n$ channels $^{160-163}$Ho behave more or less as expected for fusion-evaporation residues, the cross sections for the charged-particle channels are about two orders of magnitude higher than calculated for a complete fusion of the system ^{160}Gd+^{7}Li. This clearly indicates that another reaction mechanism is contributing to the population of these isotopes, a conclusion which is further supported by the observations discussed further below that large amounts of, in particular, deuterons and tritons are observed, and that all charged particles have considerably higher energies as in fusion-evaporation reactions and show a very strong forward-backward asymmetry. Among the charged-particle channels, ^{162}Dy is populated with the highest cross section over a very wide range of ^{7}Li beam energies between 35 and 61 MeV. The reason for this seems to be the fact that this Dy isotope is populated via three different reaction channels, namely, $p4n$, $d3n$, and $t2n$. Based on these cross-section

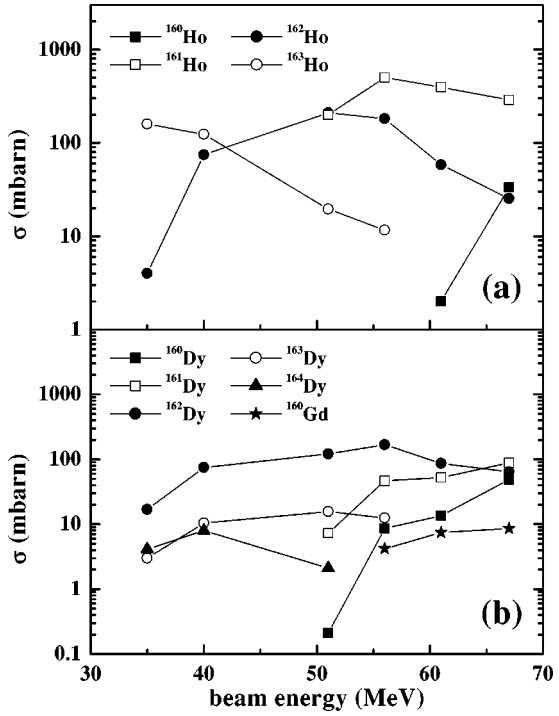

FIG. 1. Absolute cross sections in the reaction ^{7}Li+^{160}Gd for (a) the xn channels $^{160-163}$Ho and (b) the charged-particle channels $^{160-164}$Dy and ^{160}Gd.

measurements we have chosen a ^{7}Li beam energy of 56 MeV for the production runs performed at the Laboratori Nazionali di Legnaro. It is also interesting to note that the observed cross section for the excitation of the target nucleus ^{160}Gd is not due to Coulomb excitation. Protons as well as deuterons are observed in coincidence with the γ transitions in ^{160}Gd and at a beam energy of 56 MeV, excited states with spins as high as 18^{+} have been populated in this nucleus.

In Fig. 2, ΔE-E diagrams are shown, which were observed with three different Si telescopes of the ISIS ball at $\Theta = 35°$, 90°, and 120° and a beam energy of 56 MeV. Three facts are remarkable: First, the large number of detected deuterons and tritons, which are very unlikely evaporation products, second, the high energies of the protons, deuterons and tritons as reflected by the large number of particles penetrating the absorber as well as the Si detector stack, and third, the angular distributions of the charged particles, which are increasingly anisotropic the heavier the particle is. The latter is demonstrated in more detail in Fig. 3, where the yields of protons, deuterons, and tritons are shown as functions of the detection angle. As compared to the 15% anisotropy expected for particles evaporated in a fusion-evaporation reaction, forward-backward asymmetries of greater than 10, 200, and 1000 are observed for protons, deuterons, and tritons, respectively. These features are characteristic for an incomplete fusion reaction, where only part of the projectile is fusing with the target nuclei while the rest is continuing to fly in the forward direction.

The relative contributions of proton, deuteron, and triton channels in the population of $^{160-164}$Dy are shown in Fig. 4. All particles detected in the full ISIS ball were considered.

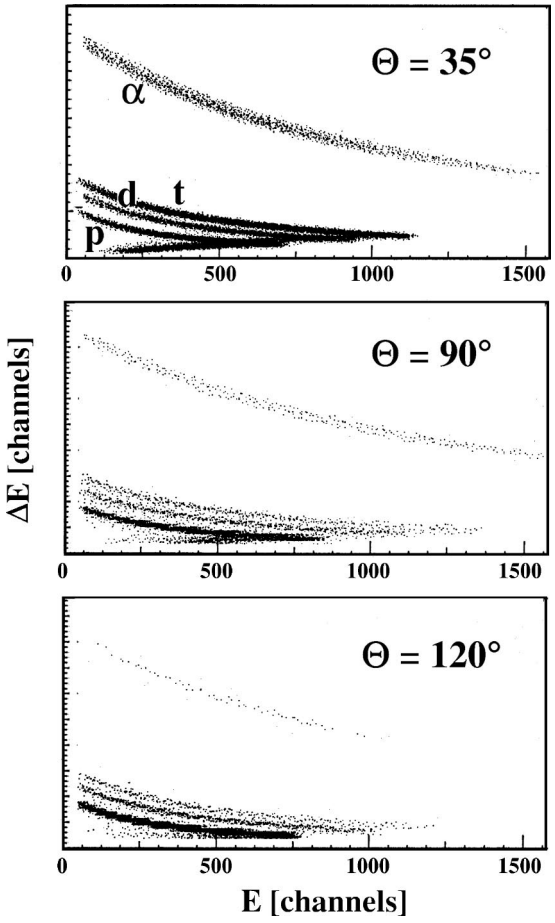

FIG. 2. ΔE-E matrices observed in three different telescopes of the ISIS Si ball, positioned at $\Theta = 35°$, 90°, and 120° with respect to the beam, in the reaction ^{7}Li+^{160}Gd at 56 MeV.

Whereas the lighter isotopes ^{160,161}Dy and the heavier ones ^{163,164}Dy are predominantly detected in coincidence with tritons and protons, respectively, the yield of ^{162}Dy in the $p4n$, $d3n$ and $t2n$ channels is comparable. It is obvious from that

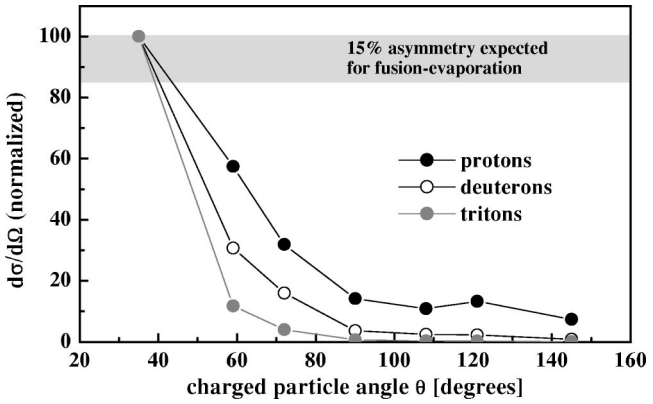

FIG. 3. Angular distribution of the hydrogen isotopes detected in the seven rings of the ISIS Si ball in the reaction ^{7}Li+^{160}Gd at 56 MeV. For comparison, a 15% anisotropy as expected from the kinematics in case of a complete fusion of the projectile with the target and a subsequent evaporation of the charged particles is indicated by a gray bar.

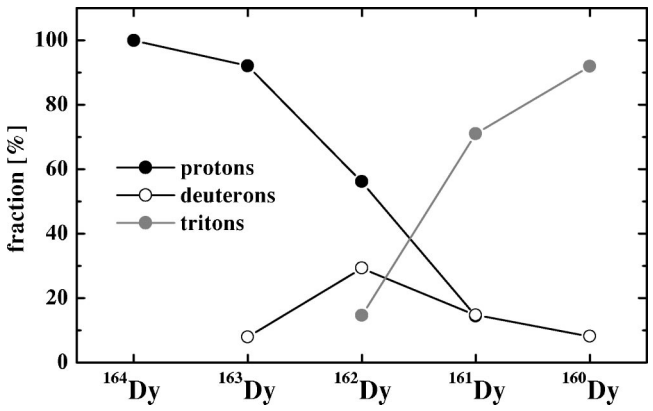

FIG. 4. Relative contributions of the three different types of charged-particle channels, namely, *p*, *d*, and *t*, to the population of the residual nuclei $^{160-164}$Dy in the reaction ^{7}Li+^{160}Gd at 56 MeV. All particles detected in the ISIS Si ball were taken into account, independent of the angle of detection.

figure that the cleanest, although not most intense, γ spectra of ^{162}Dy will be obtained in coincidence with deuterons. This selectivity and the high probability to produce neutron-rich nuclei in charged-particle reaction channels together with the high angular momentum input (states up to up to $28\hbar$ could be observed, see below) make the Li-induced reactions a very valuable tool to study the high-spin state structure in nuclei, which are not accessible in standard fusion-evaporation reactions.

IV. DATA ANALYSIS AND RESULTS FOR THE EVEN ^{160,162}Dy

To study ^{160,162}Dy at high spin, the reactions ^{158,160}Gd $(^{7}\mathrm{Li},(p,d,t)xn)$ at beam energies of 56 MeV have been employed. As discussed in detail in Sec. III, ^{162}Dy is the strongest charged-particle reaction channel using a ^{160}Gd target and, in complete analogy, ^{160}Dy is the most strongly populated one using a ^{158}Gd target. After a proper energy calibration, the events written on tape were sorted into $\gamma\gamma$ coincidence matrices. Separate matrices were created for $\gamma\gamma$ coincidences without particle condition and in coincidence with either a proton, a deuteron, or a triton being detected in one of the 40 elements of the ISIS Si ball at the same time. To build the level schemes, symmetric matrices including all 40 Ge detectors of the GASP array were created. The projections of these matrices, produced under the different gating conditions, are shown in Fig. 5 for the ^{7}Li$\rightarrow^{160}$Gd data. Although the deuteron gated spectra contain already only small contributions from ^{161,163}Dy besides the dominant ^{162}Dy lines, even cleaner ^{162}Dy spectra are obtained by gating only on the high-energy part of the deuteron spectrum. The present extensions of the level schemes of ^{160,162}Dy are mainly based on analyzing such matrices. In addition, matrices were constructed from threefold or higher gamma events with the requirement that one of the detected γ rays was one of the lowest transitions within the g.s.b. In these matrices, the g.s.b. and bands strongly decaying to it are enhanced.

To determine γ-ray multipolarities from the analysis of the directional correlation ratios from oriented states (DCO), matrices with γ rays detected in the 90° ring on one axis and γ rays observed at 35° or 145° on the other axis in coincidence with either protons or deuterons were produced. Using a coincidence gate on a stretched quadrupole transition γ_{gate}, the DCO ratio

$$R_{DCO}=\frac{I_{\gamma}(\gamma \text{ observed at } \Theta_1;\gamma_{gate} \text{ at } \Theta_2)}{I_{\gamma}(\gamma \text{ observed at } \Theta_2;\gamma_{gate} \text{ at } \Theta_1)} \times\frac{\epsilon_{\Theta_1}(\gamma)\epsilon_{\Theta_2}(\gamma_{gate})}{\epsilon_{\Theta_1}(\gamma_{gate})\epsilon_{\Theta_2}(\gamma)} \quad (1)$$

is ≈ 1 for stretched quadrupole and ≈ 0.5 for pure dipole transitions ($\Theta_1=35°$, $145°$, $\Theta_2=90°$). On the contrary, using a gate on a pure dipole transition, the expected DCO ratios for quadrupole and dipole transitions are ≈ 2 and ≈ 1, respectively. $\epsilon_{\Theta}(\gamma)$ is the relative efficiency at the energy E_{γ} of the detectors positioned at an angle Θ with respect to the beam.

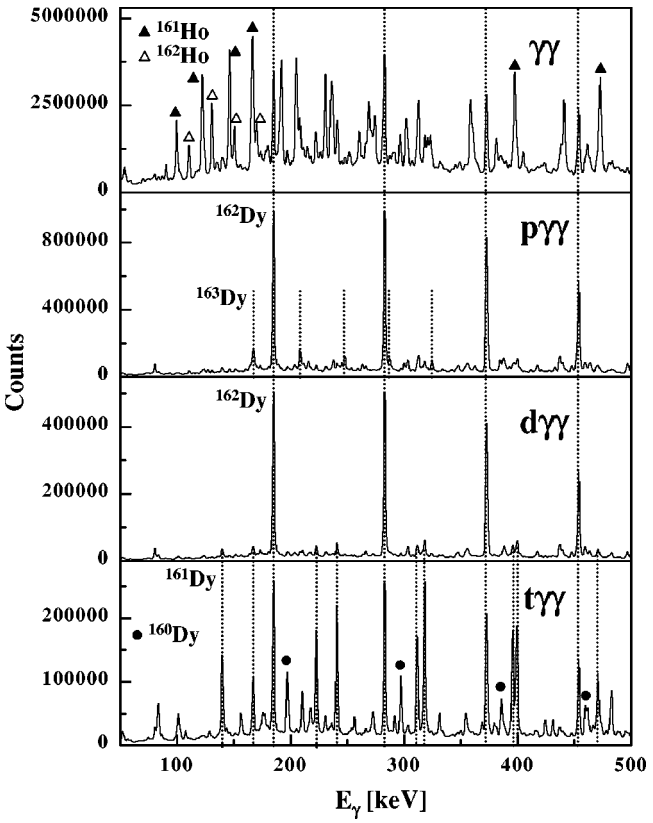

FIG. 5. Projections of the $\gamma\gamma$ matrices containing information from all Ge detectors of the GASP array (a) without particle condition and requiring the coincidence with either a proton (b), a deuteron (c), or a triton (d) for the reaction ^{7}Li$\rightarrow^{160}$Gd at 56 MeV.

A. The level scheme of ^{160}Dy

The most comprehensive study of ^{160}Dy at high spin so far has been presented by Riezebos *et al.* [19], who investigated this nucleus using the ^{158}Gd$(\alpha,\ 2n)$ reaction. In that work, the g.s.b. was established up to spin 16^{+} at around 3

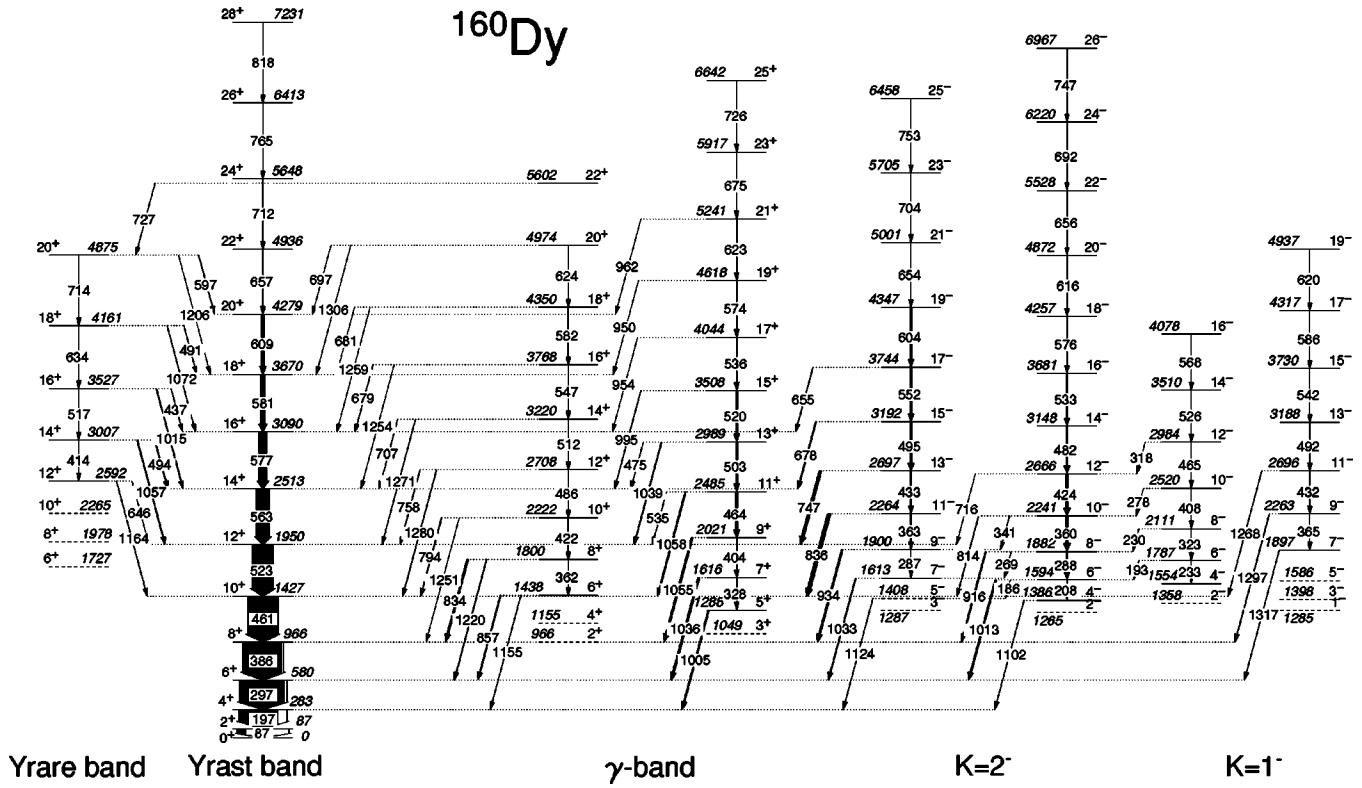

FIG. 6. Level scheme of ^{160}Dy as obtained in the present work. The low-spin members of the excited bands, which were established in previous work but not seen in our data, are shown as dashed lines.

MeV and in addition, the γ band up to the (12^+) state, some members of the Stockholm band $[(6^+)$, 8^+, and $(10^+)]$, a $K=4^+$ band and, at negative parity, $K=1^-$ [up to (10^-)], $K=2^-$ [up to (14^-)], and $K=4^-$ [up to (7^-)] bands were observed. Using the $\gamma\gamma$ coincidence information obtained as described above, we were able to extend most of the known bands to considerably higher spin as can be seen in Fig. 6, which shows the level scheme deduced in the present work. The low-spin members of the excited bands, which were established in previous work but not seen in our data, are shown as dashed lines. To illustrate the quality of the data, three coincidence spectra obtained from either the high-energy deuteron gated or the g.s.b. transition gated matrix are shown in Fig. 7. The sum of the spectra in coincidence with the 712- and 657-keV $24^+\rightarrow 22^+\rightarrow 20^+$ transitions in Fig. 7(a) gives evidence for the extension of the g.s.b. up to the 28^+ state at 7231 keV. The states at 2592, 3007, 3527, 4161, and 4875 keV are interpreted as a continuation of the yrare band, the low-spin members of which have been observed in previous work [19] (shown as dashed lines in Fig. 6). Although no γ rays connecting the new levels observed in the present work and the known low-spin members of the Stockholm band [19] could be found, two arguments support this interpretation. The first one is the very regular decay pattern, namely, the observation of two decay branches to the I and $I-2$ states of the g.s.b. for each member of the Stockholm band with spin $(6^+\leqslant I\leqslant 20^+)$ and the second one is the very smooth rotational behavior assuming all these states belonging to the same band. Figure 7(b) shows the gate on the 1072-keV transition connecting the yrast and the yrare bands.

The even and odd parts of the vibrational γ band were extended up to spin 20^+ and 25^+, respectively. All even members with spin I show a very regular decay via two branches to the I and I-2 states of the g.s.b. and the odd members decay mainly to the I-1 states of the g.s.b. The extension of the $K=2$ band at negative parity is illustrated by the sum of the coincidence spectra with gates on the 552- and 604-keV γ rays within this band shown in Fig. 7(c). All members of the $K=2^-$ band decay predominantly to the g.s.b., only the 6^-, 8^-, and 10^- states decay in addition to the I-1 levels of the $K=2^-$ band. Also the $K=1^-$ band could be considerably extended up to spin 19^-. Whereas the odd members of this band decay to the g.s.b., the decay out of the even spin states of this band proceeds via $I\rightarrow I$ transitions to the $K=2^-$ band. Finally, we would like to mention that the existence of the 4^+, 5^+, 6^+, and (7^+) states forming a $K=4^+$ band reported in [19] is confirmed by our data. However, since we have no new information on this band and it has no relevance to the following discussion, it is not included in Fig. 6, which is not intended to be a summary of all known states in this nucleus.

Very recently, Liang *et al.* [20] presented a high-spin study of ^{160}Dy using the EUROBALL IV spectrometer and the deep-inelastic reaction between a 234-MeV ^{37}Cl beam and a ^{160}Gd target. Besides the extension of the yrast band up to the 28^+ state, which is in agreement with our work, one additional sideband consisting of states with (10^+), (12^+), (14^+), (16^+), and (18^+) was established. With the help of the DCO ratios deduced as described above, these tentative spin assignments can be shown to be wrong. In Fig.

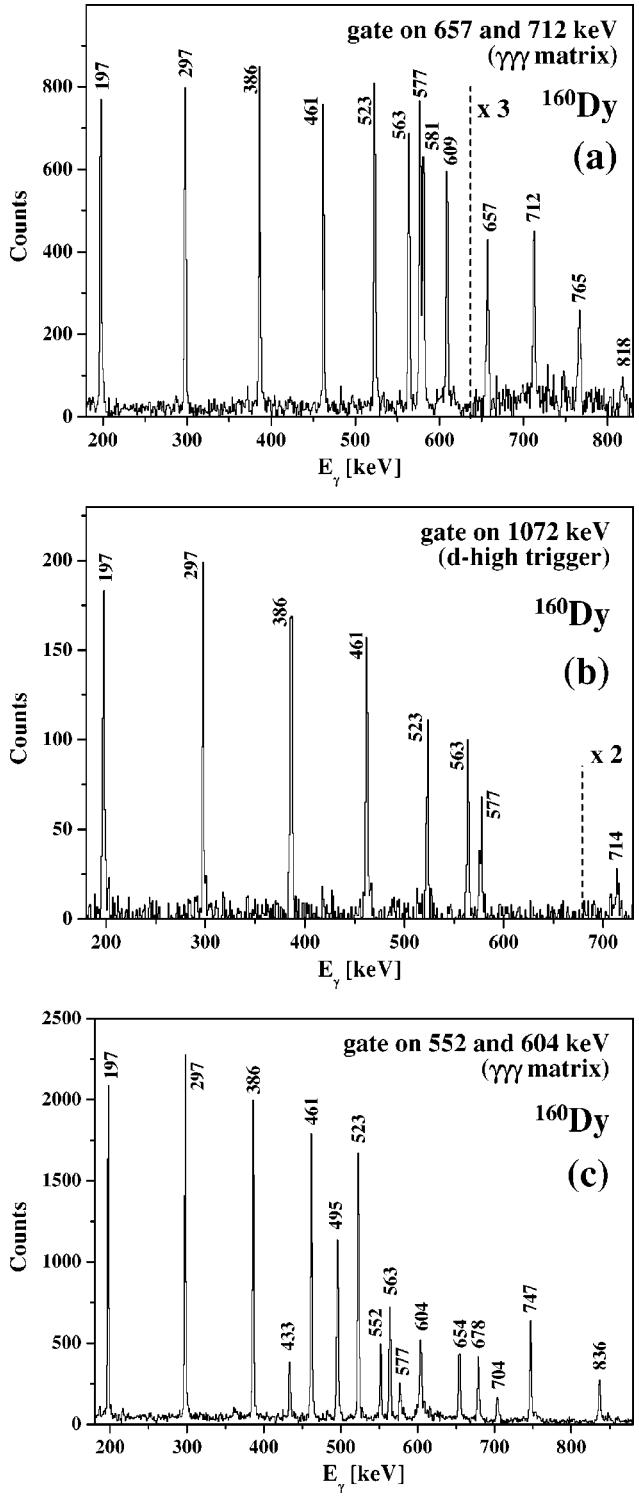

FIG. 7. Coincidence spectra obtained from either the high-energy deuteron or the g.s.b. transition gated matrix. Gates were set on the 712- and 657-keV g.s.b. transitions (a), the 1072-keV $18_2^+ \rightarrow 18_1^+$ transition (b), and the 552- and 604-keV γ rays within the $K=2^-$ band (c).

8, two spectra obtained in coincidence with the 495-keV $E2$ transition within this sequence are compared. In one case, the gating transition was observed at 35° or 145° with respect to the beam and the spectrum shown obtained at 90° and vice versa in the other case. Whereas the 523- and 563-keV g.s.b. transitions as well as the 552- and 604-keV lines have very similar intensities in both spectra, the intensities of the 747- and 836-keV transitions from the decay of the states assigned (10^+) and (12^+) in [20] clearly differ in the two spectra, roughly by a factor of 2. Both transitions are of dipole character and we assign the sequence of levels established in [20] negative parity and odd spin. Due to the observation of the 363- and 934-keV transitions, assigned in [19] as a $11^- \rightarrow 9^-$ transition within a $K=2^-$ band and a decay from the $9^-_{K=2/}$ state to the 8^+ member of the g.s.b., in coincidence with the 433- and 495-keV γ rays, we assign the 2697-, 3192-, 3744-, 4347-, 5001-, 5705-, and 6458-keV states to be the continuation of the $K=2^-$ band known from [19] (compare Fig. 6). This assignment is in agreement with all the DCO values obtained for transitions within this band and connect it to the g.s.b. The intensities and DCO ratios of all γ transitions observed in the nucleus ^{160}Dy in the present work are summarized in Table I.

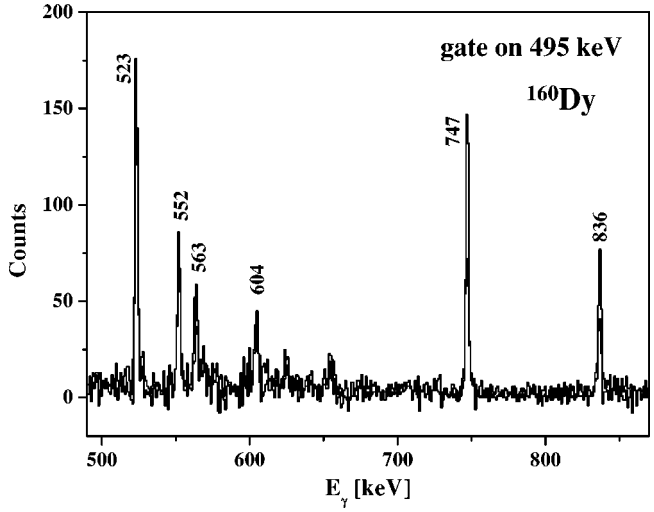

FIG. 8. Coincidence spectra with gate set on the 495-keV $E2$ transition in ^{160}Dy. The spectrum taken at 35°, 145° with the gating transition detected at 90° is shown as a black line, whereas the spectrum taken at 90° with the gating transition detected at 35°, 145° is shown as a gray line.

B. The level scheme of ^{162}Dy

Like in the case of ^{160}Dy, also for ^{162}Dy most information about the high-spin structure so far comes from an $(\alpha,2n)$ experiment [21]. In that work, a number of bands were observed up to an excitation energy of about 3.1 MeV. The g.s.b. was known up to spin 18^+ from a Coulomb excitation experiment [22]. In the experiment using deep-inelastic reactions mentioned in the preceding section, the g.s.b. was tentatively extended to a (20^+) state by placing a 741-keV $(20^+) \rightarrow 18^+$ transition [20]. Note that up to this spin, no band crossing was observed in ^{162}Dy. Unlike the case of ^{160}Dy, the Stockholm band in ^{162}Dy was known up to rather high spin, namely, the (12^+) level at 2594 keV [and tentatively a (14^+) state at 2956 keV] [21]. All bands that we were able to extend to higher spins are shown in Fig. 9. Most

TABLE I. Intensities and DCO ratios of transitions in ^{160}Dy. The intensities were determined in the sum of proton and deuteron gated spectra. Only intensities above 0.5% of I (197 keV) are given.

E_γ (keV) [a]	I_γ	R_{DCO} [b]	E_i (keV)	I_i^π	I_f^π
		Yrast band → yrast band			
196.8	1000		283	4^+	2^+
297.0	844(3)	1.12(1)	580	6^+	4^+
385.5	685(3)	1.07(1)	966	8^+	6^+
461.4	513(3)	1.03(1)	1427	10^+	8^+
522.6	359(3)	1.01(2)	1950	12^+	10^+
563.3	226(11)	1.01(2)	2513	14^+	12^+
576.5	132(7)	1.01(2)	3090	16^+	14^+
580.5	76(4)	1.01(3)	3670	18^+	16^+
608.6	47(2)	0.82(1)	4279	20^+	18^+
657.2	15(1)		4936	22^+	20^+
711.7	6(1)		5648	24^+	22^+
765.2			6413	26^+	24^+
817.8			7231	28^+	26^+
		Yrare band → yrare band			
414.3			3007	14_2^+	12_2^+
517.2			3527	16_2^+	14_2^+
634.0			4161	18_2^+	16_2^+
713.8			4875	20_2^+	18_2^+
		γ band → γ band			
362.0	7(1)		1800	8_γ^+	6_γ^+
421.6	9(1)		2222	10_γ^+	8_γ^+
486.1	5(1)		2708	12_γ^+	10_γ^+
512.2	7(1)		3220	14_γ^+	12_γ^+
547.1			3768	16_γ^+	14_γ^+
582.3	9(1)		4350	18_γ^+	16_γ^+
624.0			4974	20_γ^+	18_γ^+
328.3	5(1)		1616	7_γ^+	5_γ^+
404.2	14(1)	1.03(11)	2021	9_γ^+	7_γ^+
464.3	37(2)	1.12(7)	2485	11_γ^+	9_γ^+
503.3	22(1)		2989	13_γ^+	11_γ^+
519.7	23(1)	1.28(8)	3508	15_γ^+	13_γ^+
536.1	11(1)	0.72(6)	4044	17_γ^+	15_γ^+
574.1	12(1)		4618	19_γ^+	17_γ^+
623.0	6(1)		5241	21_γ^+	19_γ^+
675.4			5917	23_γ^+	21_γ^+
726.2			6642	25_γ^+	23_γ^+
		$K=2^-$ band → $K=2^-$ band			
286.9			1900	$9^-_{K=2^-}$	$7^-_{K=2^-}$
363.4	10(1)		2264	$11^-_{K=2^-}$	$9^-_{K=2^-}$
433.0	21(1)	1.03(6)	2697	$13^-_{K=2^-}$	$11^-_{K=2^-}$
495.4	42(2)		3192	$15^-_{K=2^-}$	$13^-_{K=2^-}$
551.5	30(2)	0.82(4)	3744	$17^-_{K=2^-}$	$15^-_{K=2^-}$
603.5	29(1)	0.80(5)	4347	$19^-_{K=2^-}$	$17^-_{K=2^-}$
653.5	8(1)		5001	$21^-_{K=2^-}$	$19^-_{K=2^-}$
703.7			5705	$23^-_{K=2^-}$	$21^-_{K=2^-}$
752.8			6458	$25^-_{K=2^-}$	$23^-_{K=2^-}$
207.9			1594	$6^-_{K=2^-}$	$4^-_{K=2^-}$
287.8	26(1)	1.12(6)	1882	$8^-_{K=2^-}$	$6^-_{K=2^-}$
359.8	44(2)	1.11(5)	2241	$10^-_{K=2^-}$	$8^-_{K=2^-}$
424.4	46(2)	1.00(3)	2666	$12^-_{K=2^-}$	$10^-_{K=2^-}$
482.2	31(2)	0.96(4)	3148	$14^-_{K=2^-}$	$12^-_{K=2^-}$
532.8	21(1)	1.01(5)	3681	$16^-_{K=2^-}$	$14^-_{K=2^-}$
575.7	13(1)	1.02(6)	4257	$18^-_{K=2^-}$	$16^-_{K=2^-}$
615.6	9(1)	1.29(9)	4872	$20^-_{K=2^-}$	$18^-_{K=2^-}$
655.6			5528	$22^-_{K=2^-}$	$20^-_{K=2^-}$
691.6			6220	$24^-_{K=2^-}$	$22^-_{K=2^-}$
746.5			6967	$26^-_{K=2^-}$	$24^-_{K=2^-}$
		$K=1^-$ band → $K=1^-$ band			
233			1787	$6^-_{K=1^-}$	$4^-_{K=1^-}$
323.2			2111	$8^-_{K=1^-}$	$6^-_{K=1^-}$
408.1			2520	$10^-_{K=1^-}$	$8^-_{K=1^-}$
465.0			2984	$12^-_{K=1^-}$	$10^-_{K=1^-}$
525.8	6(1)		3510	$14^-_{K=1^-}$	$12^-_{K=1^-}$
567.7			4078	$16^-_{K=1^-}$	$14^-_{K=1^-}$
365.3			2263	$9^-_{K=1^-}$	$7^-_{K=1^-}$
432.4			2696	$11^-_{K=1^-}$	$9^-_{K=1^-}$
491.9	6(1)		3188	$13^-_{K=1^-}$	$11^-_{K=1^-}$
542.4			3730	$15^-_{K=1^-}$	$13^-_{K=1^-}$
586.4			4317	$17^-_{K=1^-}$	$15^-_{K=1^-}$
619.8			4937	$19^-_{K=1^-}$	$17^-_{K=1^-}$
		Yrare band → yrast band			
1164.1	5(1)		2592	12_2^+	10^+
645.6			2592	12_2^+	12^+
1056.5	13(1)		3007	14_2^+	12^+
493.7	13(1)		3007	14_2^+	14^+
1014.5	10(1)	0.87(3)	3527	16_2^+	14^+
437.4		0.79(4)	3527	16_2^+	16^+
1071.7			4161	18_2^+	16^+
490.6			4161	18_2^+	18^+
1205.9			4875	20_2^+	18^+
596.7	7(1)		4875	20_2^+	20^+
		γ band → yrast band			
1154.5			1438	6_γ^+	4^+
857.3	15(1)	0.75(4)	1438	6_γ^+	6^+
1219.6	9(1)		1800	8_γ^+	6^+
834.0	28(1)		1800	8_γ^+	8^+
1251.1			2222	10_γ^+	8^+
793.8	10(1)	0.68(5)	2222	10_γ^+	10^+
1280.2	6(1)		2708	12_γ^+	10^+
757.5	6(1)	1.09(11)	2708	12_γ^+	12^+
1270.6			3220	14_γ^+	12^+
706.6			3220	14_γ^+	14^+
1253.7			3768	16_γ^+	14^+
679.0			3768	16_γ^+	16^+
1259.2			4350	18_γ^+	16^+
680.6			4350	18_γ^+	18^+
1306.2			4974	20_γ^+	18^+
696.8			4974	20_γ^+	20^+
1004.6	20(1)	0.51(3)	1288	5_γ^+	4^+
1036.0	31(2)	0.68(10)	1616	7_γ^+	6^+

TABLE I. (*Continued.*)

E_γ (keV) [a]	I_γ	R_{DCO} [b]	E_i (keV)	I_i^π	I_f^π
1054.6	29(2)	0.56(2)	2021	9^+_γ	8^+
1058.1	19(1)	0.58(3)	2485	11^+_γ	10^+
534.7		0.72(6)	2485	11^+_γ	12^+
1038.8	11(1)	0.47(3)	2989	13^+_γ	12^+
475			2989	13^+_γ	14^+
994.6			3508	15^+_γ	14^+
953.8			4044	17^+_γ	16^+
949.6			4618	19^+_γ	18^+
961.9			5241	21^+_γ	20^+
		$K=2^-$ band $\rightarrow$ yrast band			
1124.3			1408	$5^-_{K=2^-}$	4^+
1032.7	13(1)	0.46(3)	1613	$7^-_{K=2^-}$	6^+
934.1	27(1)	0.55(2)	1900	$9^-_{K=2^-}$	8^+
836.3	59(3)	0.57(4)	2264	$11^-_{K=2^-}$	10^+
747.3	45(2)	0.51(2)	2697	$13^-_{K=2^-}$	12^+
678.3	16(1)	0.67(4)	3192	$15^-_{K=2^-}$	14^+
655.2	5(1)		3744	$17^-_{K=2^-}$	16^+
1102.4			1386	$4^-_{K=2^-}$	4^+
1013.3	24(1)	1.05(6)	1594	$6^-_{K=2^-}$	6^+
185.5			1594	$6^-_{K=2^-}$	$5^-_{K=2^-}$
915.6	19(1)	0.99(6)	1882	$8^-_{K=2^-}$	8^+
268.5			1882	$8^-_{K=2^-}$	$7^-_{K=2^-}$
813.9	6(1)		2241	$10^-_{K=2^-}$	10^+
341.2			2241	$10^-_{K=2^-}$	$9^-_{K=2^-}$
715.6			2666	$12^-_{K=2^-}$	12^+
		$K=1^-$ band $\rightarrow$ $K=2^-$ band			
192.6			1787	$6^-_{K=1^-}$	$6^-_{K=2^-}$
230.0			2111	$8^-_{K=1^-}$	$8^-_{K=2^-}$
278.2			2520	$10^-_{K=1^-}$	$10^-_{K=2^-}$
318.2			2984	$12^-_{K=1^-}$	$12^-_{K=2^-}$
		$K=1^-$ band $\rightarrow$ yrast band			
1316.7			1897	$7^-_{K=1^-}$	6^+
1297.1	7(1)	0.55(5)	2263	$9^-_{K=1^-}$	8^+
1268.3			2696	$11^-_{K=1^-}$	10^+

[a]The uncertainties of the γ-ray energies are typically 0.1 keV for $E_\gamma < 1$ MeV and 0.2 keV above.
[b]R_{DCO} as defined in Eq. (1).

important is the observation of both the g.s.b. and the excited $K=0^+$ band in and above the band crossing region, allowing for the first time to determine the frequency of the delayed crossing in this nucleus and, furthermore, to deduce the interaction strengths between the two bands with a very high accuracy. To illustrate the quality of the data, the sum of the spectra obtained in coincidence with the 556- and 627-keV transitions within the Stockholm band is shown in Fig. 10(a). All transitions within this band as well as those from its decay to the g.s.b. and the γ band are visible (compare Fig. 9). Note, that the energies of the 12^+ and 14^+ states of the Stockholm band are 2534 and 2934 keV, respectively, different from the values given in [21]. Further evidence for the decay from the $K=0^+$ band to the γ band via the 312- and 447-keV γ rays, a decay branch which was not observed in ^{160}Dy, is given in Fig. 10(b), where the coincidence spectrum with a gate on the 417-keV $10^+_\gamma \rightarrow 8^+_\gamma$ transition is plotted. In complete analogy to ^{160}Dy, the γ band shows a very regular decay pattern: $I \rightarrow I$ and $I \rightarrow I$-2 transitions from the even members of the γ band to the g.s.b. and $I \rightarrow I$-1 transitions from the odd spin states. The $K=4^+$ band could be extended up to the 15^+ level. This band decays exclusively to the γ band. These results on the positive parity states are corroborated, in particular, in the spin region below 20^+ by Coulomb excitation measurements performed by the Heidelberg group [23] and more recently by Wu *et al.* [24]. Turning now to negative parity, the $K=5^-$ band, observed up to the 13^- state in [21], was extended up the the 24^- level in the present work. The spectrum obtained in coincidence with the 906-keV γ ray connecting the 11^- state of this band to the 10^+ member of the g.s.b. is shown in Fig. 10(c). In this spectrum, both rotational sequences, namely, the 402-, 463-, 521-, 577-, and 630-keV as well as the 437-, 496-, 551-, and 602-keV quadrupole transitions connecting the odd and even members of the $K=5^-$ band, respectively, can be identified. To give additional evidence for the upper part of the band, part of the coincidence spectrum of the 463-keV γ ray is plotted as an inset of Fig. 10(c). All spectra shown were obtained from the matrix sorted from triplefold or higherfold events requiring the observation of one of the four transitions between 2^+ and 10^+ in the g.s.b. The $K=5^-$ band decays mainly via the strong 906- and 782-keV dipole transitions to the 10^+ and 12^+ states of the g.s.b. Whereas the odd members of the $K=2^-$ band, which was considerably extended, too, decay via $I \rightarrow I$-1 transitions to the g.s.b., some of the even spin states of this band decay via $E1$ transitions to the γ band. Finally, the $\Delta I=2$ sequence of odd negative parity states assigned $K=(0)^-$ in [21] was observed up to spin 19^-, consisting of quadrupole inband transitions and decaying via E1 transitions to the g.s.b. The multipolarities of all γ rays were deduced from their DCO values, which are listed in Table II together with the intensities.

C. Experimental interaction strengths between ground state, Stockholm, and γ bands

The crossings of the ground state, Stockholm, and γ bands in ^{160}Dy and ^{162}Dy are clearly visible in Fig. 11, where the excitation energies are plotted as a function of $I(I+1)$. For a better visibility, the energy of a reference rotor has been subtracted from the experimental excitation energies at each spin value. In ^{160}Dy, the ground state and Stockholm bands cross around spin $I \approx 16\hbar$ ($\hbar\omega \approx 280$ keV) and the interaction between these two bands is rather strong. In ^{162}Dy, on the other hand, the interaction is weak and the crossing appears at a higher spin value of about $18\hbar$ ($\hbar\omega \approx 350$ keV). It is interesting to note that the crossing frequency in ^{162}Dy is about 70 keV higher than the frequency at which backbendings or upbendings occur in all other even-even Dy isotopes from ^{154}Dy to ^{160}Dy (all around $\hbar\omega \approx 280$ keV). The origin of this delay in the band crossing in ^{162}Dy is not yet completely understood. The interaction strength between the Stockholm and the vibrational γ bands

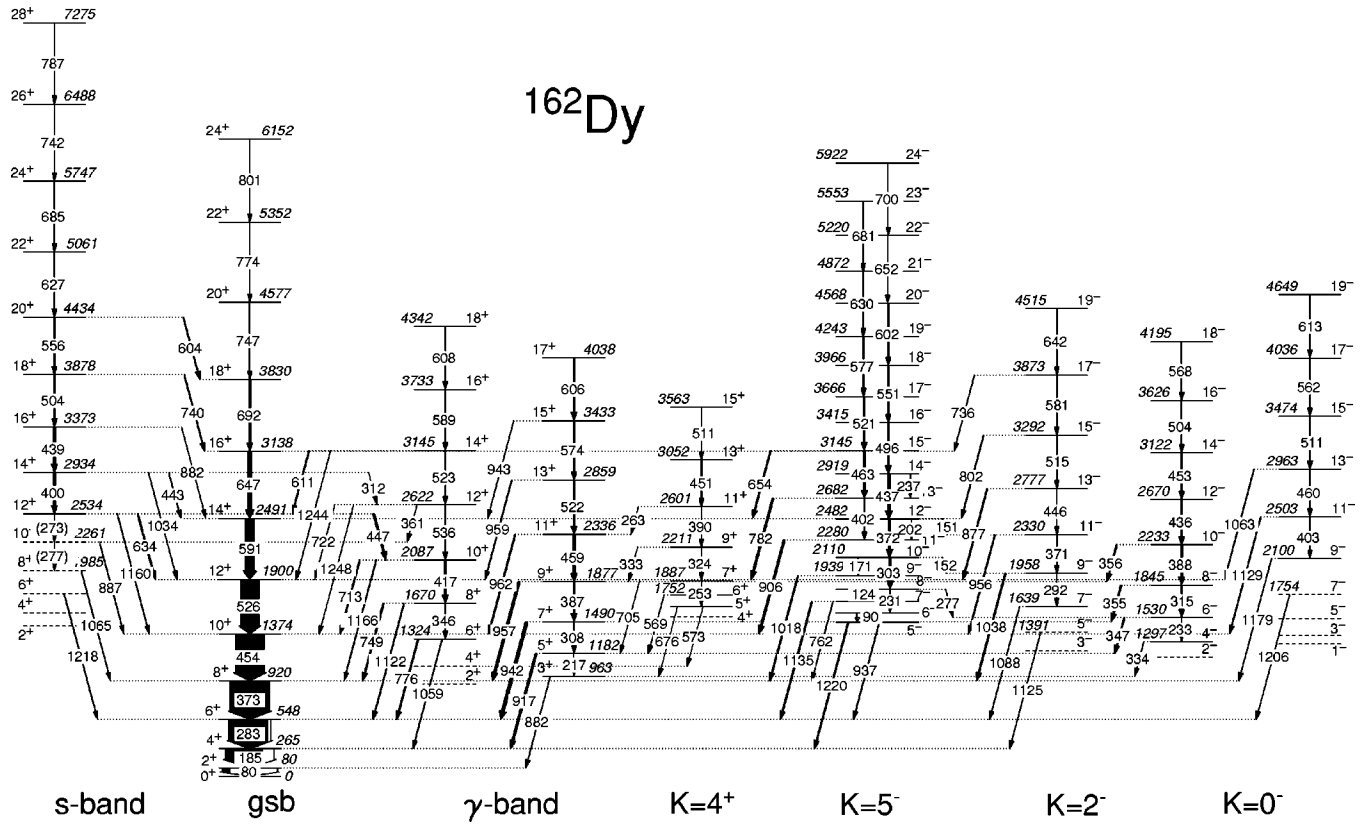

FIG. 9. Level scheme of ^{162}Dy as obtained in the present work. The low-spin members of the excited bands, which were established in previous work but not seen in our data, are shown as dashed lines.

is rather small in both nuclei with crossings around $10\hbar$ in ^{160}Dy and $12\hbar$ in ^{162}Dy. We will determine in the following the interaction strengths more precisely within a two-band-mixing model. The use of this approach seems to be legitimate considering the clear separation of the two crossing regions. We will use two different methods to determine the interaction strengths. In the first, only the excitation energies of the observed yrast and yrare states will be used. They are fitted by starting from two unperturbed rotational bands with variable moments of inertia, which interact with a strength $|V|$. In cases where relative reduced $E2$ transition rates for the γ decays to both the yrast and yrare states are known in the crossing region, this information can be used for the determination of the interaction strengths in a second approach as will be shown for the g.s.b.-Stockholm crossings later.

For the unperturbed ground state (g) and Stockholm bands (S) we adopt the parametrization from the variable moment of inertia model [25]:

$$E_b(I) = E_b^0 + \frac{I(I+1)}{2\mathcal{J}_b(I)} + \frac{1}{2}C_b(\mathcal{J}_b(I) - \mathcal{J}_b^0)^2 \qquad (2)$$

with $b = g$ or S. In this model, each rotational band is described through three parameters, namely, the excitation energy at spin $0\hbar$, E^0, the alignment parameter C, and $\mathcal{J}^0$, the moment of inertia at spin $0\hbar$. The variable moment of inertia $\mathcal{J}(I)$ is determined for each spin by minimizing the energy [$\partial E(I)/\partial\mathcal{J}(I) = 0$ for each state] and is therefore not an additional parameter. After mixing of these two unperturbed bands assuming a fixed interaction strength V, the perturbed bands

$$E_{1,2}(I) = \frac{1}{2}[E_g(I) + E_S(I) \pm \sqrt{[E_g(I) - E_S(I)]^2 + 4V^2}] \qquad (3)$$

are obtained. Here, 1,2 stand for the yrast and yrare states. In the experiment, of course only these perturbed bands are observed. One possibility to determine the interaction strength V and the six parameters $E_{g,S}^0$, $C_{g,S}$, and $\mathcal{J}_{g,S}^0$ of the unperturbed bands would be a simultaneous fit of all seven parameters to the experimental yrast and yrare level energies in the band crossing region using Eq. (3). However, such a procedure is very time consuming. Instead, we decoupled the fit of the two unperturbed bands by transforming Eq. (3) into

$$E_{g,S}(I) = \frac{1}{2}[E_1(I) + E_2(I) \pm \sqrt{\{E_1(I) - E_2(I)\}^2 - 4V^2}]. \qquad (4)$$

Now, for each value of V, the two bands are fitted separately in a spin region around the crossing and the interaction strength is obtained by searching for the χ^2 minimum of the fit. In this way, we have transformed one fit with seven parameters into two fits with three parameters each for a certain range of V values.

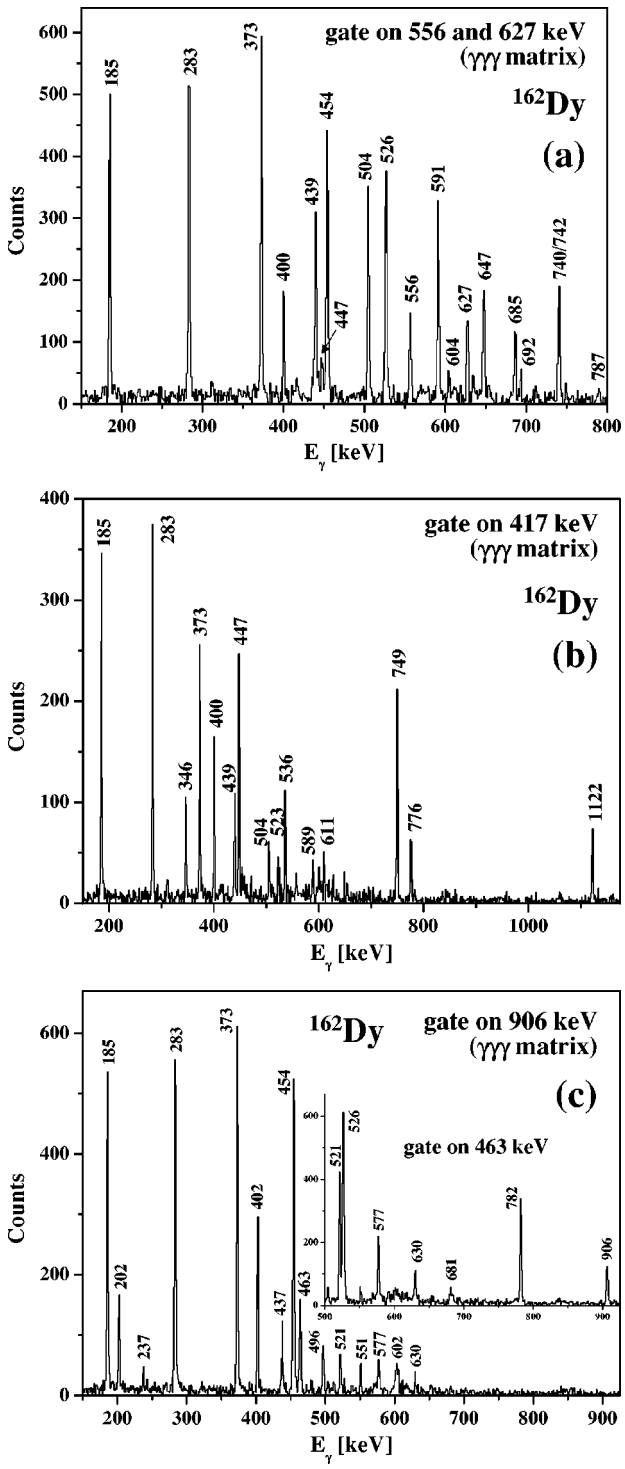

FIG. 10. Coincidence spectra obtained from the g.s.b. transition gated matrix. Gates were set on the 556- and 627-keV transitions in the Stockholm band (a), the 417-keV $10_\gamma \rightarrow 8_\gamma$ transition (b), and the 906-keV γ ray connecting the $K=5^-$ band to the g.s.b. (c). The inset of this last part shows the spectrum in coincidence with the 463-keV transition within the $K=5^-$ band.

The resulting parameters from our fits are summarized in Table III. All parameters have reasonable values. Since we do not explicitly include an alignment parameter *i* in our fit to separate between the contributions of the unpaired nucleons and the core to the total angular momentum, $\mathcal{J}^0$ is the total moment of inertia of the nucleus at spin zero as observed in the laboratory system. This total moment of inertia is larger for the Stockholm bands as compared to the ground state bands as expected. A good description of the bands over the whole spin range (not only the fit range) is obtained as shown in Figs. 12 and 13, where the experimental level energies are compared to the bands obtained in the two-band-mixing fit. On the left hand side, the whole spin range is shown, whereas on the right, the fitted, perturbed, and unperturbed bands are shown in more detail in the band crossing regions. We obtain an interaction strength of $|V_{g\text{-}S}| = 219(2)$ keV for the ground state band–Stockholm band mixing in ^{160}Dy and a value of $|V_{g\text{-}S}| = 14(2)$ keV for the same crossing in ^{162}Dy. For the γ band–Stockholm band crossings, the values are $|V_{\gamma\text{-}S}| = 13(2)$ and $|V_{\gamma\text{-}S}| = 44(2)$ keV for ^{160}Dy and ^{162}Dy, respectively.

We will now turn to the second method to determine the interaction strengths. Within the rotational model and assuming identical intrinsic quadrupole moments Q_0 for the two bands as well as the $E2$ matrix elements between the unperturbed g.s.b. and *S* band to be equal to zero, the interaction strength $|V|$ can be determined using the equation [3]

$$|V| = \frac{\sqrt{\lambda}}{1+\lambda}\Delta E_I \left[(1-R)^2 + \frac{4R\lambda}{1+\lambda} \right]^{-1/2}, \tag{5}$$

where ΔE_I is the difference in energy between the yrare and yrast states of spin *I*, $R = \Delta E_I / \Delta E_{I-2}$, and λ is the observed reduced branching ratio defined as

$$\lambda = \frac{B(E2, I_{yrare} \rightarrow [I-2]_{yrast})}{B(E2, I_{yrare} \rightarrow [I-2]_{yrare})}. \tag{6}$$

We used the γ-ray energies and branching ratios for the decay of the state at the band crossing, i.e., the 16^+ level in ^{160}Dy and the 18^+ state in ^{162}Dy. The branching ratios were determined in the most direct way, namely, in the coincidence spectra with a gate on a γ ray populating the state under study. Using $E_\gamma(16^+_{yrare} \rightarrow 14^+_{yrast}) = 1015$ keV, $b(16^+_{yrare} \rightarrow 14^+_{yrast}) = 0.648(79)$, $E_\gamma(16^+_{yrare} \rightarrow 14^+_{yrare}) = 517$ keV and $b(16^+_{yrare} \rightarrow 14^+_{yrare}) = 0.161(20)$ in ^{160}Dy and $E_\gamma(18^+_{yrare} \rightarrow 16^+_{yrast}) = 740$ keV, $b(18^+_{yrare} \rightarrow 16^+_{yrast}) = 0.386(48)$, $E_\gamma(18^+_{yrare} \rightarrow 16^+_{yrare}) = 504$ keV and $b(18^+_{yrare} \rightarrow 16^+_{yrare}) = 0.614(76)$ in ^{162}Dy, we obtain the values $|V_{g\text{-}S}| = 215(2)$ and $|V_{g\text{-}S}| = 16(2)$ keV for the g.s.b.–Stockholm band interaction in ^{160}Dy and ^{162}Dy, respectively. These values are in good agreement with those deduced from the band fit.

The interaction observed in ^{160}Dy between the g.s.b. and the *S* band is the strongest one that could be firmly established for a nucleus in the rare earth region so far. Together with the known small value for this interaction strength in ^{156}Dy and the new result for ^{162}Dy determined in the present work, a full oscillation of interaction strength in one isotopic chain in the rare earth region could now be established for the first time. This is depicted in Fig. 14, which displays the interaction strengths $|V_{g\text{-}S}|$ between the ground state and the

TABLE II. Intensities and DCO ratios of transitions in ^{162}Dy. The intensities were determined in the sum of proton and deuteron gated spectra. Only intensities above 0.5% of I (185 keV) are given.

E_γ (keV) [a]	I_γ	R_{DCO} [b]	E_i (keV)	I_i^π	I_f^π
	Ground state band → ground state band				
184.9	1000		265	4^+	2^+
282.7	913(26)		548	6^+	4^+
372.5	774(23)		920	8^+	6^+
453.6	576(17)		1374	10^+	8^+
526.2	364(11)	0.98(1)	1900	12^+	10^+
590.6	183(6)	1.01(2)	2491	14^+	12^+
647.0	89(3)	0.95(3)	3138	16^+	14^+
692.4	34(1)	1.02(5)	3830	18^+	16^+
746.8	10(1)		4577	20_2^+	18^+
774.3			5352	22_2^+	20_2^+
801.2			6152	24_2^+	22_2^+
	Stockholm band → Stockholm band				
276.6			2261	10_2^+	8_2^+
272.6			2534	12_2^+	10_2^+
399.8	38(1)	1.02(6)	2934	14_2^+	12_2^+
439.4	39(1)	1.00(6)	3373	16_2^+	14_2^+
504.4	24(1)	0.95(7)	388	18_2^+	16_2^+
556.2	17(1)	0.82(12)	4434	20^+	18_2^+
627.2	16(1)		5061	22^+	20^+
685.4	5(1)		5747	24^+	22^+
741.5			6488	26^+	24^+
787.3			7275	28^+	26^+
	γ band → γ band				
345.6	15(1)	0.98(10)	1670	8_γ^+	6_γ^+
417.0	37(1)	0.99(7)	2087	10_γ^+	8_γ^+
535.5	16(1)	0.94(9)	2622	12_γ^+	10_γ^+
523.2	14(1)		3145	14_γ^+	12_γ^+
588.6	19(1)		3733	16_γ^+	14_γ^+
608.3	11(1)		4342	18_γ^+	16_γ^+
217.3			1182	5_γ^-	3_γ^-
307.5	9(1)		1490	7_γ^-	5_γ^-
387.3	33(1)	1.05(6)	1877	9_γ^-	7_γ^-
459.1	46(2)	1.07(4)	2336	11_γ^-	9_γ^-
522.2	38(1)	0.92(5)	2859	13_γ^-	11_γ^-
574.3	28(1)	0.86(6)	3433	15_γ^-	13_γ^-
605.6	32(1)		4038	17_γ^-	15_γ^-
	$K=4^+$ band → $K=4^+$ band				
252.9			1887	$7^+_{K=4^+}$	$5^+_{K=4^+}$
323.7	6(1)		2211	$9^+_{K=4^+}$	$7^+_{K=4^+}$
389.9	6(1)		2601	$11^+_{K=4^+}$	$9^+_{K=4^+}$
451.5	15(1)		3052	$13^+_{K=4^+}$	$11^+_{K=4^+}$
511.4	6(1)		3563	$15^+_{K=4^+}$	$13^+_{K=4^+}$
	Stockholm band → ground state band				
1218.2	10(1)		1766	6_2^+	6^+
1064.6	8(1)		1985	8_2^+	8^+
887.3	10(1)		2261	10_2^+	10^+
1160.1	10(1)		2534	12_2^+	10^+
633.6	25(1)		2534	12_2^+	12^+
1033.8	6(1)		2934	14_2^+	12^+
442.7	8(1)		2934	14_2^+	14^+
882.2			3373	16_2^+	14^+
739.8	16(1)		3878	18_2^+	16^+
603.7	15(1)		4434	20^+	18^+
	γ band → ground state band				
1058.7	10(1)		1324	6_γ^+	4^+
775.8	22(1)	0.56(7)	1324	6_γ^+	6^+
1121.7	14(1)		1670	8_γ^+	6^+
749.0	27(1)	0.65(5)	1670	8_γ^+	8^+
1166.3	13(1)	0.97(9)	2087	10_γ^+	8^+
712.5	21(1)	0.59(4)	2087	10_γ^+	10^+
1247.9			2622	12_γ^+	10^+
721.7	5(1)		2622	12_γ^+	12^+
1244.2	5(1)		3145	14_γ^+	12^+
882.2	6(1)		963	3_γ^+	2^+
917.0	39(2)	0.48(2)	1182	5_γ^+	4^+
941.8	55(2)	0.56(2)	1490	7_γ^+	6^+
956.9	44(2)	0.59(4)	1877	9_γ^+	8^+
962.3	21(1)	0.62(4)	2336	11_γ^+	10^+
958.5	12(1)		2859	13_γ^+	12^+
942.5	6(1)		3433	15_γ^+	14^+
	Stockholm band → γ band				
311.6			2934	14_2^+	12_γ^+
447.3	34(1)	1.09(7)	2534	12_2^+	10_γ^+
	γ band → Stockholm band				
360.8			2622	12_γ^+	10_2^+
610.5	17(1)		3145	14_γ^+	12_2^+
	$K=4^+$ band → γ band				
675.8			1634	$5^+_{K=4^+}$	3_γ^+
573.3			1634	$5^+_{K=4^+}$	4_γ^+
569.3	5(1)		1752	$6^+_{K=4^+}$	5_γ^+
704.8			1887	$7^+_{K=4^+}$	5_γ^+
333.3			2211	$9^+_{K=4^+}$	9_γ^+
263.3			2601	$11^+_{K=4^+}$	11_γ^+
	$K=5^-$ band → $K=5^-$ band				
89.7	9(1)		1575	$6^-_{K=5^-}$	$5^-_{K=5^-}$
231.4	10(1)		1806	$8^-_{K=5^-}$	$6^-_{K=5^-}$
123.8	19(1)		1806	$8^-_{K=5^-}$	$7^-_{K=5^-}$
303.2	38(1)	1.14(6)	2110	$10^-_{K=5^-}$	$8^-_{K=5^-}$
171.0	8(1)		2110	$10^-_{K=5^-}$	$9^-_{K=5^-}$
371.9	44(2)	1.02(3)	2482	$12^-_{K=5^-}$	$10^-_{K=5^-}$
202.0	9(1)		2482	$12^-_{K=5^-}$	$11^-_{K=5^-}$
437.2	52(2)	1.02(3)	2919	$14^-_{K=5^-}$	$12^-_{K=5^-}$
237.0			2919	$14^-_{K=5^-}$	$13^-_{K=5^-}$
496.4	36(1)	1.04(5)	3415	$16^-_{K=5^-}$	$14^-_{K=5^-}$
550.7	25(1)	1.08(7)	3966	$18^-_{K=5^-}$	$16^-_{K=5^-}$
602.1	21(1)		4568	$20^-_{K=5^-}$	$18^-_{K=5^-}$
652.3	7(1)		5220	$22^-_{K=5^-}$	$20^-_{K=5^-}$
699.8			5922	$24^-_{K=5^-}$	$22^-_{K=5^-}$
402.0	15(1)	0.90(7)	2682	$13^-_{K=5^-}$	$11^-_{K=5^-}$

TABLE II. (*Continued.*)

E_γ (keV) [a]	I_γ	R_{DCO} [b]	E_i (keV)	I_i^π	I_f^π	E_γ (keV) [a]	I_γ	R_{DCO} [b]	E_i (keV)	I_i^π	I_f^π
463.2	35(1)	0.92(5)	3145	$15^-_{K=5^-}$	$13^-_{K=5^-}$	1134.6	25(1)	0.50(3)	1682	$7^-_{K=5^-}$	6^+
521.1	33(1)	1.00(6)	3666	$17^-_{K=5^-}$	$15^-_{K=5^-}$	762.0	8(1)	0.53(5)	1682	$7^-_{K=5^-}$	8^+
576.6	22(1)	1.14(9)	4243	$19^-_{K=5^-}$	$17^-_{K=5^-}$	1018.1	23(1)	0.52(3)	1939	$9^-_{K=5^-}$	8^+
629.9	13(1)		4872	$21^-_{K=5^-}$	$19^-_{K=5^-}$	905.8	37(1)	0.56(3)	2280	$11^-_{K=5^-}$	10^+
680.7	5(1)		5553	$23^-_{K=5^-}$	$21^-_{K=5^-}$	781.6	36(1)	0.51(4)	2682	$13^-_{K=5^-}$	12^+
	$K=2^-$ band $\rightarrow$ $K=2^-$ band					654.2	23(1)	0.65(4)	3145	$15^-_{K=5^-}$	14^+
232.9			1530	$6^-_{K=2^-}$	$4^-_{K=2^-}$		$K=2^-$ band $\rightarrow$ ground state band				
315.4	16(1)	0.97(7)	1845	$8^-_{K=2^-}$	$6^-_{K=2^-}$	1125.4	6(1)		1391	$5^-_{K=2^-}$	4^+
388.5	37(1)	1.06(6)	2233	$10^-_{K=2^-}$	$8^-_{K=2^-}$	1088.4	8(1)		1639	$7^-_{K=2^-}$	6^+
436.4	33(1)	0.87(5)	2670	$12^-_{K=2^-}$	$10^-_{K=2^-}$	1037.8	26(1)	0.60(3)	1958	$9^-_{K=2^-}$	8^+
452.6	17(1)	1.16(6)	3122	$14^-_{K=2^-}$	$12^-_{K=2^-}$	955.8	17(1)		2330	$11^-_{K=2^-}$	10^+
504.0	12(1)		3626	$16^-_{K=2^-}$	$14^-_{K=2^-}$	877.0	20(1)	0.55(4)	2777	$13^-_{K=2^-}$	12^+
568.3	11(1)		4194	$18^-_{K=2^-}$	$16^-_{K=2^-}$	801.6	13(1)		3292	$15^-_{K=2^-}$	14^+
291.8			1958	$9^-_{K=2^-}$	$7^-_{K=2^-}$	735.8	6(1)		3873	$17^-_{K=2^-}$	16^+
370.9	9(1)		2330	$11^-_{K=2^-}$	$9^-_{K=2^-}$		$K=0^-$ band $\rightarrow$ ground state band				
446.1			2777	$13^-_{K=2^-}$	$11^-_{K=2^-}$	1206.3	6(1)		1754	$7^-_{K=0^-}$	6^+
515.1	6(1)		3292	$15^-_{K=2^-}$	$13^-_{K=2^-}$	1179.1	7(1)		2100	$9^-_{K=0^-}$	8^+
581.0	10(1)		3873	$17^-_{K=2^-}$	$15^-_{K=2^-}$	1129.0	15(1)		2503	$11^-_{K=0^-}$	10^+
642.0	6(1)		4515	$19^-_{K=2^-}$	$17^-_{K=2^-}$	1062.6	11(1)		2963	$13^-_{K=0^-}$	12^+
	$K=0^-$ band $\rightarrow$ $K=0^-$ band						$K=2^-$ band $\rightarrow$ γ band				
403.3			2503	$11^-_{K=0^-}$	$9^-_{K=0^-}$	333.9	6(1)		1297	$4^-_{K=2^-}$	3^+_γ
460.2	11(1)		2963	$13^-_{K=0^-}$	$11^-_{K=0^-}$	347.3	22(1)	0.62(5)	1530	$6^-_{K=2^-}$	5^+_γ
510.9	17(1)		3474	$15^-_{K=0^-}$	$13^-_{K=0^-}$	355.0	28(1)	0.59(3) [c]	1845	$8^-_{K=2^-}$	7^+_γ
562.4	9(1)		4036	$17^-_{K=0^-}$	$15^-_{K=0^-}$	356.2	23(1)	0.59(3) [c]	2233	$10^-_{K=2^-}$	9^+_γ
613.3	7(1)		4649	$19^-_{K=0^-}$	$17^-_{K=0^-}$		$K=5^-$ band $\rightarrow$ $K=2^-$ band				
	$K=5^-$ band $\rightarrow$ ground state band					151.6	12(1)		2110	$10^-_{K=5^-}$	$9^-_{K=2^-}$
1220.1	21(1)	0.50(3)	1485	$5^-_{K=5^-}$	4^+	151.0	5(1)		2482	$12^-_{K=5^-}$	$11^-_{K=2^-}$
937.2	12(1)	0.54(4)	1485	$5^-_{K=5^-}$	6^+						

[a] The uncertainties of the γ-ray energies are typically 0.1 keV for $E_\gamma < 1$ MeV and 0.2 keV above.
[b] R_{DCO} as defined in Eq. (1).
[c] Common value for 355.0 and 356.2 keV doublet.

Stockholm bands for the Dy isotopes as a function of the mass number A. The interaction strengths for ^{156}Dy displayed in Fig. 14 were deduced again with the aid of Eqs. (2) and (4) using the level scheme available in the literature [26]. It agrees with the value quoted in [3]. For ^{158}Dy, where only the yrast sequence is known, $|V_{g\text{-}S}|$ could only be estimated. Also shown in Fig. 14 are the predictions for $|V_{g\text{-}S}|$ obtained within the particle-rotor model assuming axial symmetric nuclei [4], using the description given in [3] to determine the actual position of the Fermi level within the neutron $i_{13/2}$ subshell occupied by the aligned two quasiparticles in the S band, and choosing the energy scale κ to be 3 MeV as suggested in [4]. The oscillatory behavior of $|V_{g\text{-}S}|$ with A and their absolute values are reasonably well described by this calculation, and an even better agreement can be achieved by slightly adjusting the position of the Fermi level and choosing a moderately larger energy scale factor κ. An almost perfect description of the experimental interaction strength $|V_{g\text{-}S}|$ results from our projected shell-model calculations performed for ^{160,162}Dy in the following section.

V. CALCULATIONS WITHIN THE PROJECTED SHELL MODEL

The projected shell model (PSM) is a shell-model approach which starts from the deformed single-particle basis to describe rotational bands in heavy nuclei. It allows to treat heavy nuclei in a shell-model framework because important nuclear correlations are easily taken into account in a manageable configuration space. The PSM has already been used to describe the yrast lines of even-even Dy isotopes in [9] and [10]. In this work, we extend the calculations to describe in addition excited bands of both parities.

We will give only a brief reminder of the PSM here, more details can be found elsewhere [9,27–31]. The ansatz for the wave function is given by

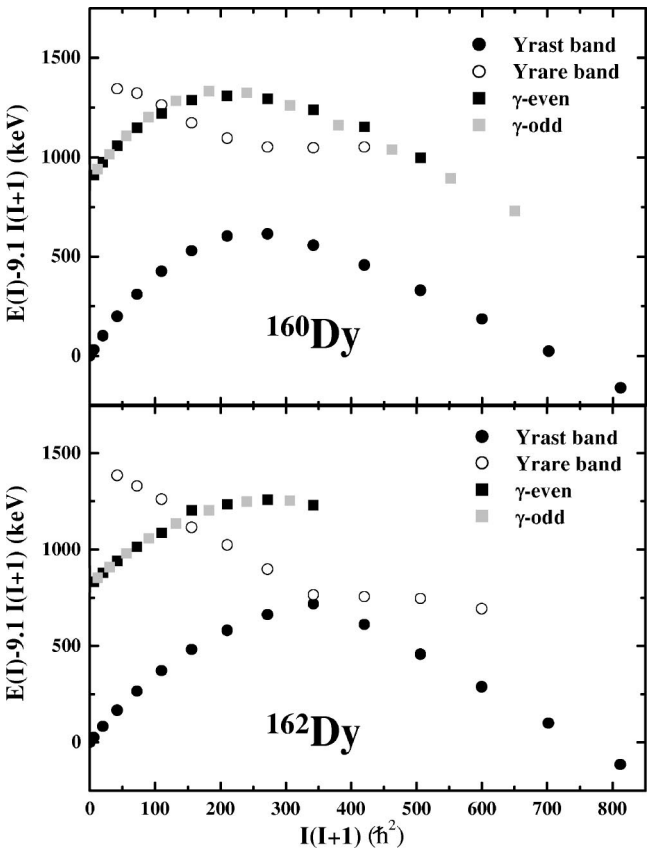

FIG. 11. Excitation energies of members of the yrast, yrare, and γ bands in ^{160}Dy (top) and ^{162}Dy (bottom) as a function of $I(I+1)$. To enhance the band crossings, the energy of a reference rotor with $E_{ref}=9.1I(I+1)$ keV has been subtracted from the level energies.

$$|\sigma,IM\rangle=\sum_{\kappa} f_{\kappa}^{\sigma}\hat{P}^{I}_{MK_{\kappa}}|\phi_{\kappa}\rangle. \tag{7}$$

The index σ labels the states with the same angular momentum and κ the basis states. The operator $\hat{P}^{I}_{MK}$ projects the quantum numbers I and M and generates states of good angular momentum, thus restoring the rotational symmetry violated in the deformed mean field. The f_{κ}^{σ} are the weights of the basis states $|\phi_{\kappa}\rangle$ which are spanned by the set

$$\{|\Phi\rangle,\alpha^{\dagger}_{n_i}\alpha^{\dagger}_{n_j}|\Phi\rangle,\alpha^{\dagger}_{p_i}\alpha^{\dagger}_{p_j}|\Phi\rangle,\alpha^{\dagger}_{n_i}\alpha^{\dagger}_{n_j}\alpha^{\dagger}_{p_k}\alpha^{\dagger}_{p_l}|\Phi\rangle\} \tag{8}$$

with $|\Phi\rangle$ a given vacuum and $\alpha_m,\alpha_m^{\dagger}$ the annihilation and creation quasiparticle operators to this vacuum. The index n_i (p_j) runs over selected neutron (proton) states around the neutron (proton) Fermi surface. These indices are general. For example, a 2-qp state can be of positive parity if both quasiparticles i and j are from the same major shell. It can also be of negative parity if the two quasiparticles are from two neighboring major shells. Positive and negative parity states span the whole configuration space with the corresponding matrix in a block-diagonal form classified by parity. In the present calculations, we have allowed active particles from three oscillator shells, $N=3,4,5$ for protons and $N=4,5,6$ for neutrons. We used the Hamiltonian

$$\hat{H}=\hat{H}_0-\frac{1}{2}\chi\sum_{\mu}\hat{Q}^{\dagger}_{\mu}\hat{Q}_{\mu}-G_M\hat{P}^{\dagger}\hat{P}-G_Q\sum_{\mu}\hat{P}^{\dagger}_{\mu}\hat{P}_{\mu}, \tag{9}$$

where $\hat{H}_0$ is the spherical single-particle shell-model Hamiltonian. The quadrupole interaction strength χ is self-consistently related to the quadrupole deformation parameter ϵ_2, which takes the value 0.29 for ^{160}Dy and 0.30 for ^{162}Dy. The monopole-pairing-force constants

$$G_M=\left(20.12\mp 13.13\frac{N-Z}{A}\right)A^{-1} \tag{10}$$

are adjusted to reproduce the known energy gaps. The minus (plus) sign applies to neutrons (protons). Finally, the strength parameter G_Q for the quadrupole pairing is taken as $0.18G_M$ for ^{160}Dy and $0.16G_M$ for ^{162}Dy. The weights f_{κ}^{σ} in Eq. (7) are determined by diagonalization of the Hamiltonian $\hat{H}'=\hat{H}-\lambda\hat{N}$ in the space spanned by the states of Eq. (8), with $\hat{N}$ the particle number operator. This leads for a given spin to the eigenvalue equation

TABLE III. Results of the two-band-mixing calculations for the g.s.b.–Stockholm band and γ band–Stockholm band interactions in ^{160,162}Dy.

Band	Spin range ($\hbar$)	$\lvert V\rvert$ (keV)	$\mathcal{J}^0$ ($\hbar^2$ MeV^{-1})	C (MeV$^3\hbar^4$)	E^0 (MeV)
			^{160}Dy		
g.s.b.	14–20	219(2)	32.8	0.004	0.01
Stockholm	14–20	219(2)	69.8	0.094	1.37
γ band	6–14	13(2)	33.9	0.002	0.88
Stockholm	6–14	13(2)	62.5	0.004	1.4
			^{162}Dy		
g.s.b.	16–22	14(2)	35.8	0.004	0.02
Stockholm	16–22	14(2)	69.0	0.2	1.4
γ band	8–16	44(2)	40.0	0.004	0.83
Stockholm	8–16	44(2)	68.8	0.006	1.46

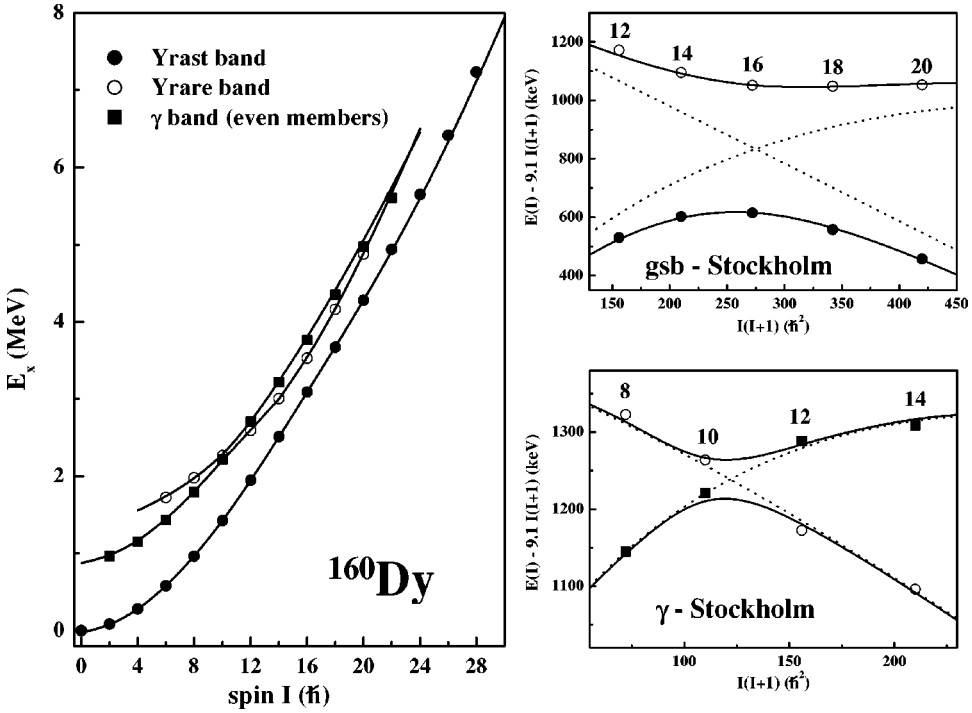

FIG. 12. Experimental level energies of the yrast, yrare, and γ (even members only) bands in ^{160}Dy in comparison with the fits obtained in the two-band mixing model (see text for details). On the right, the g.s.b.–Stockholm band and γ band–Stockholm band crossing regions are shown enlarged. The dashed lines indicate the unperturbed ground state and Stockholm bands, and the full lines indicate the yrast and yrare bands obtained in the two-band-mixing fit.

$$\sum_{\kappa'} (\mathcal{H}'_{\kappa\kappa'} - E_\sigma \mathcal{N}_{\kappa\kappa'}) f^\sigma_{\kappa'} = 0 \tag{11}$$

with

$$\mathcal{H}'_{\kappa\kappa'} = \langle \phi_\kappa | \hat{H}' \hat{P}_{K_\kappa K'_{\kappa'}} | \phi_{\kappa'} \rangle \quad \text{and}$$

$$\mathcal{N}'_{\kappa\kappa'} = \langle \phi_\kappa | \hat{P}_{K_\kappa K'_{\kappa'}} | \phi_{\kappa'} \rangle .$$

The normalization is chosen such that

$$\sum_{\kappa\kappa'} f^\sigma_\kappa \mathcal{N}_{\kappa\kappa'} f^{\sigma'}_{\kappa'} = \delta_{\sigma\sigma'} . \tag{12}$$

Since one of the basic ideas of the shell model is that the same Hamiltonian should describe all the nuclear states in a given nucleus, we would like to point out that the theoretical bands discussed in the following sections for either ^{160}Dy or ^{162}Dy are obtained by one single diagonalization for each nucleus without adjusting any parameters for individual states. In practice, one can use certain symmetries to simplify the diagonalization procedure. For example, matrix elements of positive and negative parity states have a block-diagonal form because there is no coupling between these two groups.

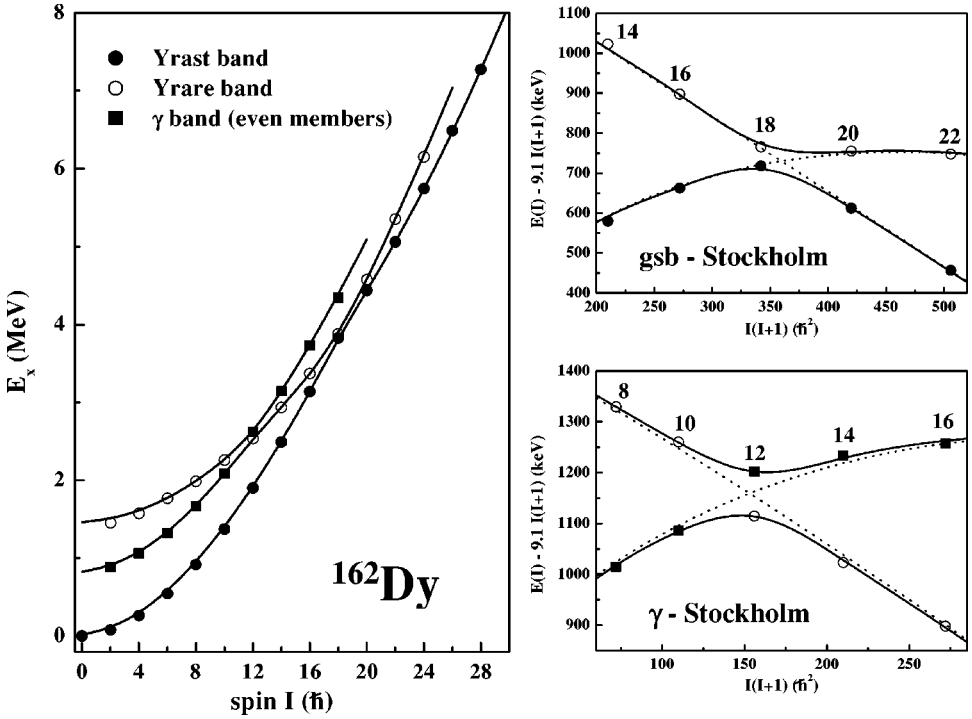

FIG. 13. Experimental level energies of the yrast, yrare, and γ (even members only) bands in ^{162}Dy in comparison with the fits obtained in the two-band-mixing model (see text for details). On the right, the g.s.b.–Stockholm band and γ band–Stockholm band crossing regions are shown enlarged. The dashed lines indicate the unperturbed ground state and Stockholm bands, and the full lines indicate the yrast and yrare bands obtained in the two-band mixing fit.

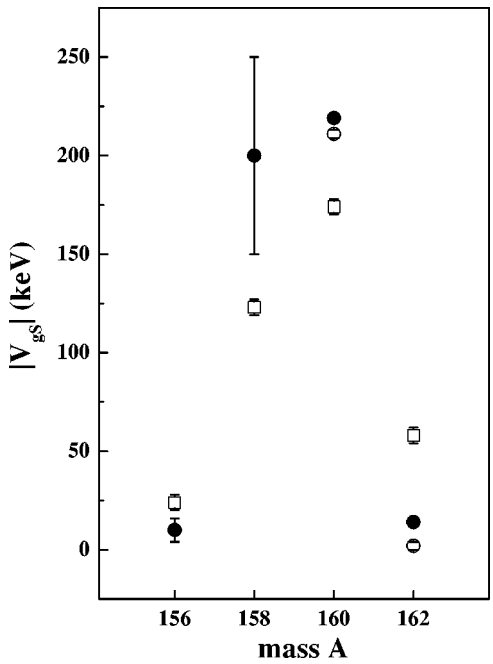

FIG. 14. Interaction strengths for the g.s.b.–Stockholm band crossings in the even-even Dy isotopes. The filled circles present the experimental values, the open squares are predictions within the particle-rotor model (see also main text), whereas the open circles are the values obtained in the PSM calculations (see Sec. V).

Therefore, diagonalization can be carried out separately within smaller spaces. The calculation of the γ bands was done in the triaxial PSM [31], which requires all possible intrinsic K states besides $K=0$ to be included. However, it has been shown [31] that for well-deformed nuclei like those discussed here, intrinsic K states with $K\neq 0$ have very little influence on the ground state and quasiparticle states based on it. That is, the nucleus exhibits an axial symmetry. Therefore, it is unnecessary to include these components for the yrast and yrare band calculations.

The lowest eigenstates of Eq. (11) provide a theoretical approach to the excitation energies of the nuclei we are interested in. Since the basis states $|\phi_\kappa\rangle$ of Eq. (8) are eigenstates of the parity operator, the solutions of Eq. (11)—the states $|\sigma,IM\rangle$—are eigenstates, too. The positive (negative) parity eigenstates are obtained by diagonalization of Eq. (11) within the corresponding basis states.

The angular momentum projected 2-qp states are defined by $E_\kappa(I)=\mathcal{H}'_{\kappa\kappa}/\mathcal{N}_{\kappa\kappa}$. A plot of these states as a function of I indicates the configurations involved in the crossing between the g.s.b. and the S band before the band mixing of Eq. (11). We found from the PSM calculation that the S bands have main components of the configurations coupled from the high-j orbitals. For ^{160}Dy, two neutron $i_{13/2}$ orbitals with $K=3/2$ and 5/2 lie near the Fermi level. Their coupling to the 2-qp $K=1$ band is the main component of the ^{160}Dy S band. For ^{162}Dy, three neutron $i_{13/2}$ orbitals with $K=3/2$, 5/2, and 7/2 are close to the Fermi level. The low-energy 2-qp states can be coupled from these orbitals as ($K=3/2$, $K=5/2$) and ($K=5/2$,$K=7/2$), both having a total $K=1$. We found that the S band in ^{162}Dy is a mixture of these two configurations.

In Fig. 15 we present the comparison between the theoretical results (lines) and the experimental data (symbols) for the positive parity bands. For the yrast band of ^{160}Dy, the agreement with experiment is very good, only in the upbending region (see inset) a slight deviation is observed. The theoretical yrare states are also in good agreement with the experiment. For spin values smaller than $14\hbar$ we do not pro-

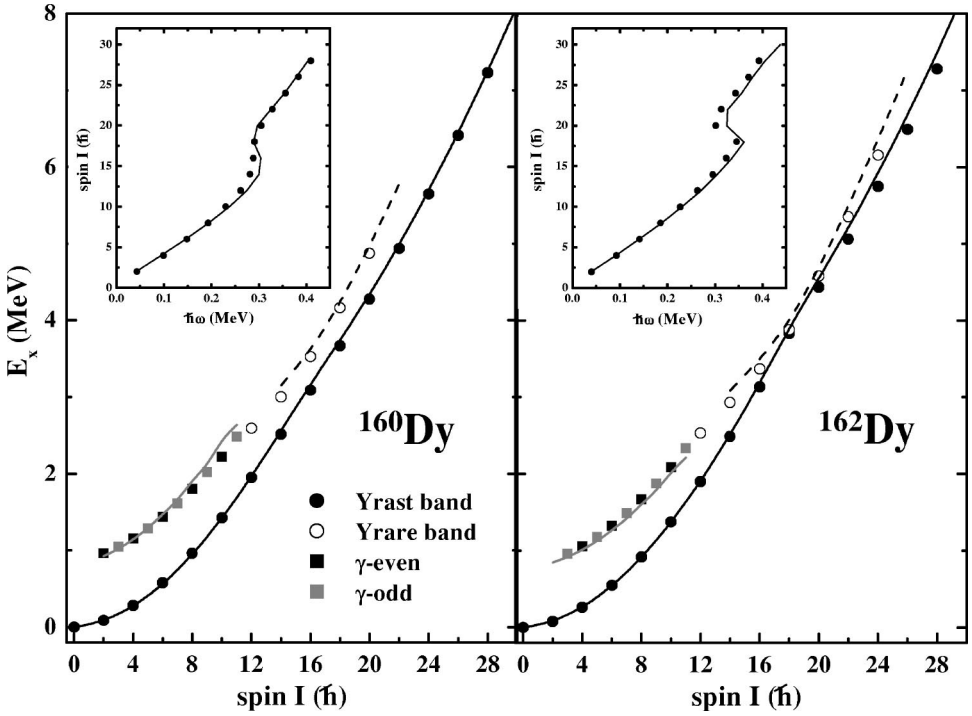

FIG. 15. Comparison between the experimental excitation energies and the results of the PSM calculations for the yrast, yrare, and γ bands in ^{160}Dy (left) and ^{162}Dy (right). Filled and open circles mark the experimental yrast and yrare bands and black and gray squares mark the two signatures of the experimental γ band. The theoretical results are shown as solid, dashed, and solid gray lines for the yrast, yrare, and γ bands. In the insets, both experimental and calculated yrast lines are shown in a backbending plot.

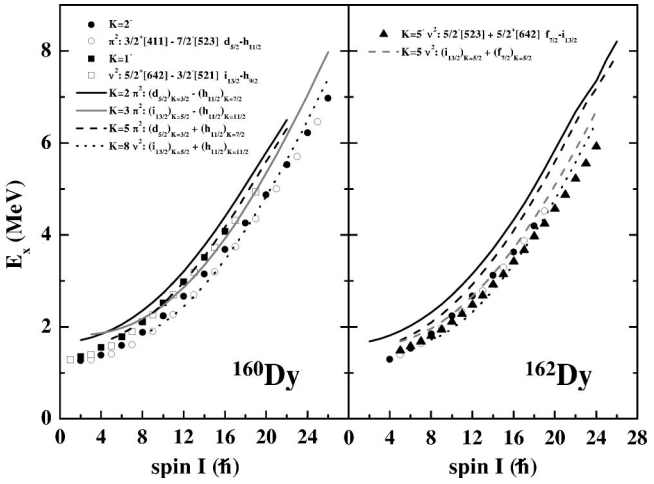

FIG. 16. Comparison between the experimental excitation energies and the results of the PSM calculations for the negative parity bands in ^{160}Dy (left) and ^{162}Dy (right). The experimentally observed states are shown as symbols (circles, squares, and triangles for the $K=2^-$, $K=1^-$, and $K=5^-$ bands, respectively) and the theoretical results as lines. The theoretical curves are labeled by the dominating 2-qp configuration.

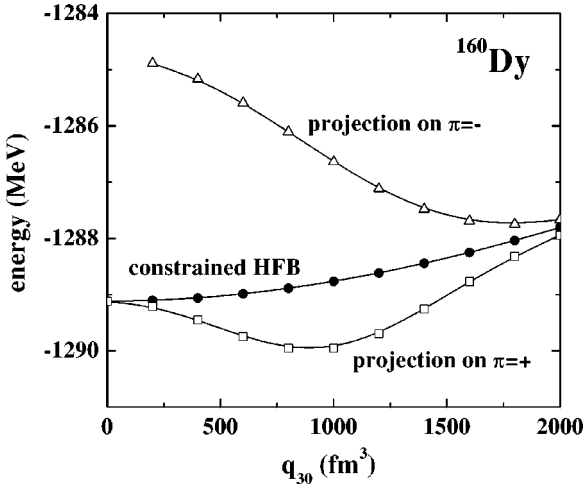

FIG. 17. Energy of the nucleus ^{160}Dy as a function of the octupole deformation parameter q_{30} in different approximations: In the constrained, parity nonconserving, Hartree-Fock-Bogoliubov calculations, filled circles, and in the negative (positive) parity projected HFB solutions, open triangles (squares) (see text for details).

vide any states because it is difficult to identify them due to the high level density present at these excitation energies. The γ band is also well described by the theory, especially at low spin where the band is rather pure. At higher spins, after crossing with other bands, it is more difficult to describe it properly due to the mixing with other bands (see [32]). For ^{162}Dy, the theoretical predictions for the yrast band agree very well with the data for spin values below the backbending. The quality of the agreement is not as good above the backbending but as it can be seen in the inset, the backbending is very well reproduced. The yrare and the γ bands are also well described by the theory.

In Fig. 16 we present the comparison between the theoretical results (lines) and the experimental data (symbols) for the negative parity bands. It is not possible to find an exact one-to-one correspondence between theory and experiment. A possible explanation for the discrepancy will be given below. The lowest theoretical band heads are characterized by the following configurations. For ^{160}Dy, the two neutron orbitals $i_{13/2}$ $(K=5/2)$ and $h_{11/2}$ $(K=11/2)$ lie near the neutron Fermi level, while the two proton orbitals $d_{5/2}$ $(K=3/2)$ and $h_{11/2}$ $(K=7/2)$ are close to the proton Fermi level. The pair of neutron orbitals can couple to two 2-qp states with $K=3$ and 8, and the pair of proton orbitals can couple to two 2-qp states with $K=2$ and 5. The theoretical results in Fig. 16 are a mixture of all these 2-qp states (and others lying higher in energy). After the band mixing, we can still mark our theoretical bands by one particular configuration if it is dominated by it. For ^{162}Dy, the three neutron orbitals $i_{13/2}$ $(K=5/2)$, $f_{7/2}$ $(K=5/2)$, and $h_{11/2}$ $(K=11/2)$ lie near the neutron Fermi level while the two proton orbitals $d_{5/2}$ $(K=3/2)$ and $h_{11/2}$ $(K=7/2)$ are close to the proton Fermi level, like in the case of ^{160}Dy. Thus, the pair of proton orbitals can couple to two 2-qp states with $K=2$ and 5. There are more possibilities for the neutron coupling. We found, however, that the lowest two are $i_{13/2}$ $(K=5/2)+f_{7/2}$ $(K=5/2)$ coupled to $K=5$ and $i_{13/2}$ $(K=5/2)+h_{11/2}$ $(K=11/2)$ coupled to $K=8$. Again, the theoretical negative parity bands in Fig. 16 are the mixture of them.

A possible explanation for the discrepancy in the quality of the theoretical predictions for the positive and the negative parity bands could be the fact that these nuclei are rather soft against octupole fluctuations. Unfortunately, the pairing plus quadrupole model Hamiltonian does not have this degree of freedom and it is not possible to check the effect of considering octupole deformed basis states on the different observables. To investigate this point we have performed calculations with the density dependent finite range Gogny force [33], which allows for octupole deformations, and gives a good description of nuclei where this degree of freedom has turned out to be important [34]. To study the softness against octupole deformations, we have performed Hartree-Fock-Bogoliubov (HFB) calculations with a constraint on the octupole operator q_{30} for the nucleus ^{160}Dy. In Fig. 17 we present the binding energy of the nucleus as a function of q_{30} calculated in the HFB approach (filled circles). We do not find an octupole deformed nucleus but a very soft one, it takes little more than 1 MeV to deform the nucleus from $q_{30}=0$ to $q_{30}=2000$ fm^3. The octupole constrained HFB calculations do not provide eigenstates of the parity operator and should be considered in this respect as intrinsic wave functions. To restore the parity symmetry one must project onto this quantum number out of the HFB wave functions. The binding energy calculated with the projected wave functions (see [35]) is represented by open squares (positive parity) and open triangles (negative parity). From these curves we find that positive and negative states have the minimum binding energy at very different q_{30} values, i.e., the intrinsic wave function for the positive party states has an octupole deformation of about 1000 fm^3, while that for negative parity has 1800 fm^3. Since the parameters that enter the pairing plus quadrupole Hamiltonian have been adjusted to describe

optimally the positive parity states, one does not wonder why the agreement with the experiment is better for these states than for the negative parity ones.

VI. CONCLUSIONS

The heavy stable rare earth nuclei ^{160,162}Dy were studied using the incomplete fusion reactions $^{7}\mathrm{Li}\rightarrow{}^{158,160}$Gd at beam energies of 56 MeV. The known rotational bands in both nuclei could be extended by about 84 new states to higher spins. One of the most important achievements of the present work is the observation of the yrare band in ^{160}Dy up to high spin, namely, the $I=20\hbar$ level, which allowed to accurately determine the interaction strength between the ground state band and the Stockholm band, $|V_{g\text{-}S}|=219(2)$ keV. This is the strongest interaction firmly established for a nucleus in the rare earth region yet. With $|V_{g\text{-}S}|=14(2)$ keV determined in the present work for ^{162}Dy and the values for ^{156,158}Dy known from literature, a full oscillation of the ground state band–Stockholm band interaction strengths was observed for the first time within a single isotopic chain. In ^{162}Dy, we were able to observe the long searched for delayed backbending at a crossing frequency of $\hbar\omega\approx 350$ keV. This crossing occurs at a much higher frequency as compared to other nuclei in this mass region. The new experimental information were compared to calculations within the projected shell model. Whereas very good agreement was obtained for the positive parity bands, the quality of the description of the negative parity bands is unsatisfactory. One possible reason for that might be the neglection of the octupole degree of freedom in the PSM calculations, which HFB calculations using the Gogny force predict to play an important role at negative parity.

ACKNOWLEDGMENTS

We are most grateful to the crews of the tandem accelerators at the LNL Legnaro and the MPI Heidelberg for their friendly and efficient cooperation. This work has been supported by Deutsches Bundesministerium für Bildung, Wissenschaft, Forschung und Technologie (BMBF). A.J. acknowledges support by the Deutsche Forschungsgemeinschaft (DFG).

[1] R. Bengtsson, I. Hamamoto, and B. Mottelson, Phys. Lett. **73B**, 259 (1978).
[2] R. Bengtsson and S. Frauendorf, Nucl. Phys. **A314**, 27 (1979).
[3] G. B. Hagemann and I. Hamamoto, Phys. Rev. C **46**, 838 (1992).
[4] I. Hamamoto, Phys. Lett. B **179**, 327 (1986).
[5] J. Almberger, I. Hamamoto, and G. Leander, Phys. Lett. **80B**, 153 (1979).
[6] G. D. Dracoulis, A. P. Byrne, T. Kibedi, T. R. McGoram, and S. M. Mullins, J. Phys. G **23**, 1191 (1997).
[7] K. Siwek-Wilczynska, E. H. du Marchie van Voorthuysen, J. van Popta, R. H. Siemssen, and J. Wilczynski, Nucl. Phys. **A330**, 150 (1979).
[8] D. R. Haenni, T. T. Sugihara, R. P. Schmitt, G. Mouchaty, and U. Garg, Phys. Rev. C **25**, 1699 (1982).
[9] Y. Sun and J. L. Egido, Nucl. Phys. **A580**, 1 (1994).
[10] V. Velazques, J. G. Hirsch, Y. Sun, and M. W. Guidry, Nucl. Phys. **A653**, 355 (1999).
[11] T. Härtlein, H. Bauer, B. Binder, A. Dietrich, Ch. Gund, D. Pansegrau, D. Schwalm, A. Jungclaus, G. B. Hagemann, G. de Angelis, E. Farnea, A. Gadea, D. R. Napoli, D. Bazzacco, C. Rossi Alvarez, S. Lunardi, and C. Ur, Nuovo Cimento **111**, 645 (1998).
[12] A. Jungclaus, B. Binder, A. Dietrich, T. Härtlein, H. Bauer, Ch. Gund, D. Pansegrau, D. Schwalm, D. Bazzacco, G. de Angelis, E. Farnea, A. Gadea, S. Lunardi, D. R. Napoli, C. Rossi Alvarez, C. Ur, and G. B. Hagemann, Prog. Part. Nucl. Phys. **46**, 213 (2001).
[13] A. Dietrich, diploma thesis, Universität Heidelberg, 1998.
[14] C. Rossi Alvarez, Nucl. Phys. News **3**, 10 (1993).
[15] E. Farnea, G. de Angelis, M. De Poli, D. De Acuna, A. Gadea, D. R. Napoli, P. Spolaore, A. Buscemi, R. Zenon, R. Isocrate, D. Bazzacco, C. Rossi Alvarez, P. Pavan, A. M. Bizzeti-Sona, and P. G. Bizzeti, Nucl. Instrum. Methods Phys. Res. A **400**, 87 (1997).
[16] B. Binder, diploma thesis, Universität Heidelberg, 1998.
[17] G. Basbas, W. Brandt, and R. Laubert, Phys. Rev. A **7**, 983 (1973).
[18] F. D. Mc Daniel, T. J. Gray, R. K. Gardner, G. M. Light, J. L. Duggan, H. A. van Rinsvelt, R. D. Lear, G. H. Pepper, J. W. Nelson, and A. R. Zander, Phys. Rev. A **12**, 1271 (1975).
[19] H. J. Riezebos, M. J. A. de Voigt, C. A. Fields, X. W. Cheng, R. J. Peterson, G. B. Hagemann, and A. Stolk, Nucl. Phys. **A465**, 1 (1987).
[20] X. Liang, R. Chapman, K.-M. Spohr, M. B. Smith, P. Bednarczyk, S. Naguleswaran, F. Haas, G. de Angelis, S. M. Campbell, P. J. Dagnall, M. Davison, G. Duchene, Th. Kröll, S. Lunardi, and D. J. Middleton, Eur. Phys. J. A **10**, 41 (2001).
[21] C. A. Fields, K. H. Hicks, R. A. Ristinen, F. W. N. de Boer, P. M. Walker, J. Borggreen, and L. K. Peker, Nucl. Phys. **A389**, 218 (1982).
[22] M. W. Guidry, I. Y. Lee, N. R. Johnson, P. A. Butler, D. Cline, P. Colombani, R. M. Diamond, and F. S. Stephens, Phys. Rev. C **20**, 1814 (1979).
[23] H. Bauer, Ph.D. thesis, Universität Heidelberg, 1998.
[24] C. Y. Wu, D. Cline, M. W. Simon, G. A. Davis, R. Teng, A. O. Macchiavelli, and K. Vetter, Phys. Rev. C **64**, 064317 (2001).
[25] M. A. J. Mariscotti, G. Scharff-Goldhaber, and B. Buck, Phys. Rev. **178**, 1864 (1969).
[26] R. B. Firestone, *Table of Isotopes* (Wiley-Interscience, New York, 1996).
[27] K. Hara and S. Iwasaki, Nucl. Phys. **A348**, 200 (1980).

[28] K. Hara and Y. Sun, Nucl. Phys. **A529**, 445 (1991).
[29] K. Hara and Y. Sun, Int. J. Mod. Phys. E **4**, 637 (1995).
[30] J. A. Sheikh and K. Hara, Phys. Rev. Lett. **82**, 3968 (1999).
[31] Y. Sun, K. Hara, J. A. Sheikh, J. G. Hirsch, V. Velazques, and M. Guidry, Phys. Rev. C **61**, 064323 (2000).
[32] J. L. Egido, H. J. Mang, and P. Ring, Nucl. Phys. **A339**, 390 (1980).
[33] D. Gogny, in *Nuclear Selfconsistent Fields*, edited by G. Ripka and M. Porneuf (North-Holland, Amsterdam, 1975).
[34] J. L. Egido and L. M. Robledo, Nucl. Phys. **A494**, 85 (1989); **A518**, 475 (1990).
[35] E. Garrote, J. L. Egido, and L. M. Robledo, Phys. Rev. Lett. **80**, 4398 (1998).